Hydrogenation of CO/CO_2 mixtures under unsteady-state conditions: Effect of the carbon oxides on the dynamic methanation process

*Dominik Meyer, Jens Friedland, Jannik Schumacher, Max G. Gäßler, Robert Güttel**

Institute of Chemical Engineering, Ulm University,

Albert-Einstein-Allee 11, 89081 Ulm, Germany

*Corresponding author:

E-mail address: robert.guettel@uni-ulm.de

Abstract

The Power-to-Gas (PtG) process offers the opportunity to store fluctuating renewable energy in form of chemical energy by hydrogenating carbon oxides into methane. In addition, potential carbon point sources often consist of CO/CO_2 (CO_x) mixtures. Hence, reactor design requires kinetic models valid for unsteady-state operation and a broad spectrum of feed gas compositions. In order to provide the required experimental data basis for derivation of kinetic expressions valid under transient conditions, the dynamic response of a continuously operated fixed-bed methanation reactor is studied by applying periodic step-changes in the feed composition. The obtained results are evaluated based on a simple reactor model, providing the molar flow rate exchanged between the gas bulk and the solid surface for CO, CO_2, CH_4, and H_2O. The results further reveal that the transient kinetic processes at the catalyst surface strongly affect the reactor response under reaction conditions of technical relevance.

Keywords

- Experimental investigation
- Transient behavior
- Step-response
- Simulation based data evaluation
- Methanation
- Periodic experiments

List of Symbols

Symbol	Description	Unit
Latin letters		
d_p	Particle size	µm
F	Step response	1
f	Activity factor	1
m_cat	Catalyst mass	mg
N_Θ	Number of limit cycles	1
$\dot{n}$	Molar flow rate	mol s^{-1}
$\bar{\dot{n}}$	Average molar flow rate	mol s^{-1}
n	Molar amount of component	mol
p	Operating or partial pressure	bar
R	Universal gas constant	J mol^{-1} K^{-1}
r	Reaction rate	mol kg^{-1} s^{-1}
s	Cycle split	1
T	Operating temperature	K
t	Time	s
$\dot{V}$	Volumetric flow rate	mL_{STP} min^{-1}
x	Molar fraction	1
z	CO/CO_2 feed ratio	1
Greek letters		
α	Volume variation factor	1
Θ_C	Carbon surface coverage	1
ν	Stoichiometric coefficient	1
τ	Period duration	s
Subscripts		
+ / -	Desorbed / re-adsorbed	
1, 2	Initial / final steady-state	
dil	Dilution	
fit	Fit	
i	Component A_i	
in	Inlet	
j	Reaction R_j	
m	Number of limit cycle	
out	Outlet	
RTD	Residence time distribution	
ref	Reference	
STP	Standard temperature pressure	
ss	Steady-state	
trans	Transient	

Abbreviations	
CO_x	CO/CO_2
PtG	Power-to-Gas
RTD	Residence time distribution

1 Introduction

The Power-to-X process is a promising technology to tackle the challenge of the storage of surplus fluctuating renewable electricity by converting it into chemical energy. During the Power-to-Gas (PtG) process, H_2 is produced from water and renewable electrical energy via electrolysis and subsequently converted with the carbon oxides CO or CO_2 into CH_4 (synthetic natural gas) by the Sabatier reactions (Götz et al., 2016; Rönsch et al., 2016; Kalz et al., 2017). In short and mid-term, the most promising carbon oxide sources are industrial exhaust gases, such as blast-furnace and converter gas from steel industry, gases from cement production or biomass gasification, which potentially consist of CO/CO_2 (CO_x) mixtures of variable composition over time (Sutton et al., 2001; Schöß et al., 2014; Uribe-Soto et al., 2017). Using highly concentrated CO_2 from those sources also offers to reduce industrial CO_2 emissions significantly. In perspective, this technology can be applied to achieve negative emissions, as well, if CO_2 from ambient air is used as reactant (House et al., 2011; Goeppert et al., 2012; Dittmeyer et al., 2019). Such point sources for renewable energy and carbon oxides require local PtG plants in order to avoid costly transport infrastructure and inefficiencies in distribution (Vogt et al., 2019). This also requires plants at a smaller scale tailored to the local availability of the carbon and energy resources. Due to economic reasons such small scale plants, though, probably exhibit small buffer capacities to dampen fluctuations originating from renewable resources (Vogt et al., 2019; Theurich et al., 2020). Consequently, the methanation reactor is supplied by a dynamically changing feed gas mixture and flow rate, which needs the reactor to be operated in an unsteady-state mode. In order to design and operate methanation reactors efficiently and safely under unsteady-state CO_x methanation conditions detailed knowledge on the dynamics of this process upon changes in the H_2/CO_x feed gas composition is necessary.

The exothermic hydrogenation of CO and CO_2 into CH_4 (eqs. (1) and (2)) is performed by means of a porous catalyst, being Ni/Al_2O_3 the most common compound (Gao et al., 2015). Other metals, such as Co, Ru and Fe are also found to be active and selective, but are only rarely applied commercially so far (Mills and Steffgen, 1974; Gao et al., 2015). The most important side reactions are the reverse water gas shift reaction (RWGS) (eq. (3)), as well as the Boudouard reaction (eq. (4)). The RWGS provides some flexibility towards changes in the feed gas mixture, as it allows to adjust the ratio between CO, CO_2 and H_2 to stoichiometrically favored values. In addition to that the feed gas composition imposes kinetic effects, as well, since CO is known to strongly inhibit the CO_2 methanation process (Inui et al., 1980; Weatherbee and Bartholomew, 1982; Meyer et al., 2020). The Bouduard reaction leads to coke formation, which might cause deactivation of the catalyst. Further minor reactions involved are summarized by Miao et al. (Miao et al., 2016) together with a comprehensive overview of the relevant mechanistic aspects for CO and CO_2 methanation.

$$\mathrm{CO_2 + 4H_2 \rightleftharpoons CH_4 + 2\,H_2O} \qquad \Delta H_\mathrm{R}^{298\mathrm{K}} = -164\ \mathrm{kJ\ mol^{-1}} \tag{1}$$

$$\mathrm{CO + 3H_2 \rightleftharpoons CH_4 + H_2O} \qquad \Delta H_\mathrm{R}^{298\mathrm{K}} = -205\ \mathrm{kJ\ mol^{-1}} \tag{2}$$

$$\mathrm{CO_2 + H_2 \rightleftharpoons CO + H_2O} \qquad \Delta H_\mathrm{R}^{298\mathrm{K}} = 41\ \mathrm{kJ\ mol^{-1}} \tag{3}$$

$$\mathrm{2\,CO \rightleftharpoons CO_2 + C} \qquad \Delta H_\mathrm{R}^{298\mathrm{K}} = -172\ \mathrm{kJ\ mol^{-1}} \tag{4}$$

Dynamically changing feed gas compositions, also designated as concentration forcing, induces an unsteady-state response of the reactor on form of transient behavior of the outlet composition (Bailey et al., 1971; Renken, 1972; Matros, 1987; Marković et al., 2008; Güttel, 2013; Hudgins et al., 2013). Interestingly, different length scales relevant for heterogeneously catalyzed reactions contribute to this response, namely the macro or reactor scale, the meso or pellet scale and the micro scale for processes related to the active surface (Güttel et al., 2020). Most recent studies concentrate on the theoretical investigation of the unsteady-state reactor behavior for CO and CO_2 methanation by means of modeling and simulation. Emphasis is on temperature control (Li et al., 2015; Try et al., 2017; Bremer and Sundmacher, 2019; Kreitz et al., 2019b; Theurich et al., 2020), optimal reactor (Kiewidt and Thöming, 2015; Kreitz et al., 2019b; Fischer and Freund, 2020) or catalyst (Zimmermann et al., 2020) design, and possible performance enhancement (Currie et al., 2018; Nikačević et al., 2020), since the

exothermic methanation is limited by thermodynamic constraints at higher temperatures and puts high demands for safe operation. Those studies, however, rely on reaction kinetics obtained under steady-state conditions, which are not suitable to investigate the reactor behavior under highly dynamic conditions, as will be shown in the present contribution. The reason is that the reactor response is not only governed by residence time distribution, but kinetic processes at the catalyst surface, e.g. ad- and desorption of reacting species, become relevant. In other words, since steady-state kinetics assume equilibrium conditions at the catalyst surface, the respective kinetic processes involved are neglected. In contrast to this assumption, a dynamic and complex system at the catalyst surface arises contributing to the unsteady-state reactor behavior, which requires appropriate consideration of those kinetic processes in the reactor model.

Several experimental studies towards the effect of concentration forcing on the dynamic reactor response for methanation have already been performed at the micro and macro scale (Yadav and Rinker, 1990; Adesina et al., 1995; Klusáček and Stuchlý, 1995; Kreitz et al., 2019a). At the macro scale Stiegler et al. (Stiegler et al., 2019) and Theurich et al. (Theurich et al., 2020) recently demonstrated experimentally that improved temperature control of an unsteady-state methanation reactor is possible in structured reactors system (Stiegler et al., 2019) or by product recirculation (Theurich et al., 2020). With focus at the micro scale one of the first studies was performed by Van Ho and Harriott (Van Ho, 1980) reporting that the CH_4 response differs for CO_2 and CO methanation. The authors observed a slow exponential decline of CH_4 content at the reactor outlet after a switch from a CO_2 rich to a CO_2 free feed, indicating hydrogenation of an unreactive carbon component during the CO_2 free phase. In contrast for CO containing feeds, they reported a rapid increase in the formation rate of CH_4, when the CO containing feed is switched off. Underwood and Bennet (Underwood and Bennett, 1984) demonstrated that this behavior is caused by a reactive carbon species adsorbed at the surface. Later, Efstathiou and Bennet (Efstathiou and Bennett, 1989) expanded this work and showed that also an inactive species is hydrogenated to CH_4 when the feed is switched from being CO rich to CO free. Moreover, Yadav and Rinker (Yadav and Rinker, 1992) explained that the CH_4 behavior after switches from a CO containing to pure H_2 feed is mainly determined by the applied H_2/CO molar ratio in the CO

rich phase. Fujita et. al. (Fujita et al., 1993) conducted diffusive reflectance infrared Fourier-transform spectroscopy (DRIFTS) measurements for the unsteady-state CO and CO_2 methanation and suggested that the highly reactive species only exists in combination with strongly adsorbed bridged CO. Based on these observations different reaction mechanisms were proposed to describe the unsteady-state CO and CO_2 methanation process, which includes the formation of CO as an intermediate species for the CO_2 reaction path (Stuchlý and Klusáček, 1993; Marwood et al., 1994; Aparicio, 1997). In all these studies, however, the CH_4 response is evaluated only. Therefore, no conclusion can be drawn on the interplay of the transient behavior of all reactants detected in the gas phase. In contrast, Bundhoo et al. (Bundhoo et al., 2009) considered all reactants for the unsteady-state CO methanation reaction and provide the dynamic O, H and C mass balances. Based on that they concluded that the availability of metallic sites for hydrogen influences the CH_4 response mostly. However, the unsteady-state methanation reaction was only studied either for CO or CO_2 methanation. The dynamics of the methanation of CO_x mixtures has not been reported so far, neither studied experimentally, nor by modeling and simulation.

Consequently, the present contribution aims at closing the gap between unsteady-state CO and CO_2 methanation experimentally under realistic conditions by applying the novel periodic transient kinetics (PTK) method introduced recently by Meyer et al. (2021). The PTK method is based on the chemical transient kinetics (CTK) method (Raub et al., 2021) and utilizes periodic step-changes between two different feed-gas mixtures in order to induce a periodic transient reactor response. The resulting limit cycle, obtained for each individual component, is statistically analyzed in order to derive an average transient response with improved significance. Furthermore, an internal standard is used to measure the residence time distribution (RTD) in each single experiment *in situ*. By evaluating the obtained response with a simple unsteady-state reactor model the molar flow rate exchanged between the gas bulk and the solid surface for each individual component is derived as function of time within the limit cycle. As pointed out by Meyer et al. (2021) this methodology provides the basis to separate kinetic processes at the macro scale (e.g., RTD) from those at the micro scale (surface reaction steps) experimentally and is demonstrated to be applicable to realistic reaction conditions. The present

contribution, hence, exploits the capabilities of the PTK method for derivation of mechanistic insights under transient conditions using CO_x methanation as an example.

In particular, we put emphasis on the influence of the CO/CO_2 ratio at constant H_2/CO_x ratio on the transient response. Therefore, a carbon rich feed stream consisting of a particular CO_x ratio between pure CO and pure CO_2 is exchanged with a carbon free stream by step-shaped periodical switching at the reactor inlet. The transient response of the isothermal reactor is monitored for the most relevant carbonaceous species (i.e., CO, CO_2, CH_4) and H_2O at the outlet. Additionally, an unsteady-state reactor model is applied based on steady-state reaction kinetics developed for the CO_x methanation reaction (Meyer et al., 2020), in order to evaluate the experimental data. The applied experimental procedure and model-based evaluation enables us to investigate the processes at the catalyst surface without superimposed RTD effects. We are thereby able to link the kinetic processes at the catalyst scale to the unsteady-state reactor behavior. Furthermore, we show that the transient CH_4 response depends not only on the kinetic processes of this species at the catalyst surface but also on the transient behavior of the other reactants. It is further revealed that steady-state reaction kinetics are not sufficient to describe the dynamic reactor behavior for fast changes of the inlet composition.

2 Materials and Methods

2.1 Catalyst

The catalyst based on 5 wt-% Ni/A_2O_3 with a particle size of 150 – 200 µm is synthesized via an incipient wetness method. By means of H_2 chemisorption and N_2 physisorption measurements (3Flex, Micromeritics) the specific surface area (Brunauer-Emmett-Teller) of 168 $m^2\ g^{-1}$ with an average pore diameter of 8 nm and the H_2 adsorption capacity of 48 µmol g^{-1} are obtained. Assuming spherical Ni nanoparticles as well as an adsorption stoichiometry of two for H_2 a crystallite size of 7.5 nm, a metal surface area of 3.7 $m^2\ g^{-1}$, and a metal dispersion of 14.2 % is determined. More information about the catalyst synthesis and characterization procedure can be found in our previous publication (Meyer et al., 2020).

2.2 Experimental Setup

For all experiments a stainless-steel fixed bed reactor with an inner diameter of 4.5 mm and a total length of 30 cm is used, in which 50 mg of the catalyst sample diluted with 100 mg of inert material (200 µm, Al_2O_3, Sasol Puralox) is placed in the center of the isothermal zone. For fixation of the packing 1.2 g glass particles (150 – 200 µm) are used above (ca. 5 cm length) and 0.6 g below (ca. 2.5 cm length) the catalyst packing. The whole packing is framed by quartz wool. The reactor is fed by two separate supply lines, which can be automatically switched by means of a 4/2 way-valve (Fitok, BOSS-4C). The continuous supply of the gases is provided from top of the reactor with separate mass flow controllers (EL-FLOW Prestige, Bronkhorst) for each gas and each supply line. The feed gas compositions in both gas lines can be individually adjusted with the reactants H_2 (5.0 purity, MTI), CO/Ar (90 vol.-% CO 3.8 purity in Ar 5.0 purity, Air Liquide) and CO_2 (4.8 purity, MTI), the internal standard Ar (5.0 purity, MTI) and the inert component He (5.0 purity, MTI). Directly at the reactor outlet the gas flow can be diluted with a mixture of H_2 and Ne (both 5.0 purity, MTI) prior entering the analytics. The analytics consist of a gas chromatograph (GC-2010, Shimadzu) and a mass spectrometer (MS, Cirrus 3-XD, MKS). The MS analyzes following species by calibrated mass-to-charge ratios quantitatively: 2 (H_2), 15 (CH_4), 18 (H_2O), 28 (CO and CO_2), 40 (Ar), and 44 (CO_2). The calibration of H_2O is done *in situ* with pure CO methanation reaction at 556 K, since significant side reactions are proven to be absent under these conditions (Meyer et al., 2020). Additionally, the mass-to-charge ratios for higher hydrocarbons 26 (C_2H_6 and C_3H_8) and 43 (C_3H_8) are measured qualitatively. A flowsheet of the experimental setup is given in the supplementary information (see SI, Figure S1) and a more detailed description of the experimental setup can be found elsewhere (Meyer et al., 2021).

2.3 Experimental Procedure

The experiments are performed at different temperatures and CO_x feed ratios with the same catalyst sample under the conditions given in Table 1 and Table 2. Prior to the experiments the catalyst is reduced *in situ* at 673 K for 12 h under flowing H_2 (50 mL_{STP} min^{-1}). Between each experiment the catalyst was conditioned for 1 h under flowing H_2 (125 mL_{STP} min^{-1}) at 603 K in order to ensure an

identical initial state, which is verified by reproduction of the first experiment after three consecutive experiments with negligible deviations only (see SI, Figure S2).

Table 1: Operating conditions.

Parameter	Symbol	Unit	Value
Catalyst mass	m_{cat}	mg	50
Particle size	d_{p}	µm	200
Total inlet flow rate	$\dot{V}_{\mathrm{in,STP}}$	mL_{STP} min^{-1}	250
Dilution flow rate (H_2/Ne)	$\dot{V}_{\mathrm{dil,STP}}$	mL_{STP} min^{-1}	245/5
Operating temperature	T	K	513 – 576
Operating pressure	p	bar	2
Period duration	τ	s	240
Split	s	1	0.5

For concentration forcing experiments the H_2/He feed gas mixture is periodically exchanged with the CO_x/H_2/He/Ar mixture by step-shaped switching between feed line 1 and 2 according to Table 2. In each experiment 50 periods are performed. The respective experiments are carried out for different CO_x ratios as defined by the parameter z (eq. (5)), where $z = 0$ corresponds to pure CO_2 methanation and $z = 1$ to pure CO methanation. The half-period after the switch from H_2/He to CO_x/H_2/He/Ar is denominated as build-up phase, while the other half-period is referred to as back-transient phase.

$$z = \frac{p_{\mathrm{CO,in}}}{p_{\mathrm{ref}}} = 1 - \frac{p_{\mathrm{CO_2,in}}}{p_{\mathrm{ref}}} \tag{5}$$

The reference partial pressure is set constant to $p_{\mathrm{ref}} = 0.2\ \mathrm{bar}$, which corresponds to the constant CO_x partial pressure in all experiments. Furthermore, the partial pressure of H_2 and the CO_x/H_2 ratio is kept constant in all experiments. Note that the reactor is operated in differential mode according to Shekhtman and Yablonsky (Shekhtman and Yablonsky, 2005) in all experiments by keeping the total carbon oxide conversion below 10 %.

Table 2: Inlet partial pressures $\mathrm{p}_{i,\mathrm{in}}$ for component A_i in feed line 1 and 2.

A_i	$\mathrm{p}_{i,\mathrm{in}}$ / bar	$\mathrm{p}_{i,\mathrm{in}}$ / bar
Feed line	1	2
He	0.98	1.20
$\mathrm{H_2}$	0.80	0.80

CO_x	0.20	0
Ar	0.02	0

2.4 Model-based data evaluation

2.4.1 Calculation of molar flow rates

Neon (Ne) is used as external standard by dosing it into the reactor outlet stream with a constant molar flow rate $\dot{n}_{\mathrm{Ne}}$. Hence, the measured Ne signal x_{Ne} is only affected by changes in the overall molar flow rate at the outlet $\dot{n}_{\mathrm{out}}$ (eq. (6)). By comparison of the measured molar fraction x_{Ne} under reaction conditions with the reference obtained under absence of reaction $x_{\mathrm{Ne,ref}}$, parameter α can be derived with eq. (7). The parameter α is used in order to quantify the outlet molar flow rate $\dot{n}_{i,\mathrm{out}}$ from the measured molar fraction $x_{i,\mathrm{out}}$ of component A_i with eq. (8). $\dot{V}_{\mathrm{in,STP}}$ represents the overall inlet volumetric flow rate under standard temperature T_{STP} and pressure p_{STP}; R is the universal gas constant.

$$x_{\mathrm{Ne}}(t) = \frac{\dot{n}_{\mathrm{Ne}}}{\dot{n}_{\mathrm{out}}(t)} \tag{6}$$

$$\alpha(t) = \frac{x_{\mathrm{Ne,ref}}}{x_{\mathrm{Ne}}(t)} = \frac{\dot{n}_{\mathrm{out}}(t)}{\dot{n}_{\mathrm{out,ref}}} \tag{7}$$

$$\dot{n}_{i,\mathrm{out}}(t) = \alpha(t)\, x_{i,\mathrm{out}}(t) \frac{p_{\mathrm{STP}}\, \dot{V}_{\mathrm{in,STP}}}{R\, T_{\mathrm{STP}}} \tag{8}$$

The evaluation of the transient behavior of the components is performed based on the PTK method, which is described in detail elsewhere (Meyer et al., 2021). Therefore, the outlet molar flow rate $\dot{n}_{i,m}$ of component A_i is measured during consecutive limit cycles m first. Afterwards, the average limit cycle in terms of outlet molar flow rate $\bar{\dot{n}}_{i,\mathrm{out}}$ for all measured compounds is derived by using data for $N_\Theta = 25$ limit cycles according to eq. (9). Figure S3 (see SI) illustrates a representative average limit cycle at 556 K and $z = 0.5$. Due to the very narrow standard deviation interval (shaded areas), we will only show the average values in the following figures for sake of clarity.

$$\bar{\dot{n}}_{i,\mathrm{out}}(t) = \frac{1}{N_\Theta} \sum_{m=1}^{N_\Theta} \dot{n}_{i,m,\mathrm{out}}(t) \tag{9}$$

The unsteady-state behavior of each component is determined to some extent by transport processes at different length scales. As the internal standard (Ar) does not interact with the catalyst surface, its transient behavior depicts all transport processes on reactor and particle scale. Hence, the internal standard represents the residence time distribution (RTD) of the system. Any deviation from the Ar response, thus, indicates the interaction of the respective component A_i with the catalyst surface. By normalizing the measured outlet molar flow rate $\dot{n}_{i,\mathrm{out}}$ with the values of its initial ($\dot{n}_{i,\mathrm{ss},1}$) and final steady-state ($\dot{n}_{i,\mathrm{ss},2}$), the step response F_i can be derived for each component A_i according to eq. (10).

$$F_i(t) = \frac{\dot{n}_{i,\mathrm{out}}(t) - \dot{n}_{i,\mathrm{out,ss},1}}{\dot{n}_{i,\mathrm{out,ss},2} - \dot{n}_{i,\mathrm{out,ss},1}} \tag{10}$$

Based on the step response of the internal standard F_{Ar} the expected transient behavior of the outlet molar flow rate of each component $\dot{n}_{i,\mathrm{RTD}}$ governed by RTD of the reactor only can thus be derived according to eq. (11). The deviation of the measured outlet molar flow rate of each component $\dot{n}_{i,\mathrm{out}}$ from the expected RTD during a transient process can be quantified by eq. (12) and is assigned to the transient molar flow rate $\dot{n}_{i,\mathrm{trans}}$. Since the obtained RTD is equal for all species, the transient molar flow rate characterizes processes involved at the catalyst surface. Note, the reference molar flow rates $\dot{n}_{\mathrm{i,out,ss},2}$ are given in the SI (Table S1).

$$\dot{n}_{i,\mathrm{RTD}}(t) = F_{\mathrm{Ar}}(t)(\dot{n}_{i,\mathrm{out,ss},2} - \dot{n}_{i,\mathrm{out,ss},1}) + \dot{n}_{i,\mathrm{out,ss},1} \tag{11}$$

$$\dot{n}_{i,\mathrm{out}}\,(t) = \dot{n}_{i,\mathrm{RTD}}(t) + \dot{n}_{i,\mathrm{trans}}(t) \tag{12}$$

2.4.2 Model description

In order to evaluate the experimental results an unsteady-state, quasi-homogeneous plug-flow reactor model is applied accounting for the change in molar amount with reaction extent (eq. (13)). The molar flow rate $\dot{n}_i$ is assumed to change along the axial direction x, due to chemical reaction.

$$\frac{\partial n_i}{\partial t} = \frac{\partial \dot{n}_i}{\partial x}\mathrm{d}x + \mathrm{d}m_{\mathrm{cat}}(\nu_{i,\mathrm{CO}}\, r_{\mathrm{CO}} + \nu_{i,\mathrm{CO_2}}\, r_{\mathrm{CO_2}}) \tag{13}$$

The reaction kinetics used to calculate the mass specific reaction rate r_j for CO and CO_2 methanation are taken from our previous study, which is performed with the same catalyst (Meyer et al., 2020) and given in the SI (eq. (S1) and (S2)). It is important to emphasize that the model is thus not capable to

predict dynamic processes at the catalyst surface. Therefore, any transient process on the catalyst scale causes a deviation between simulated and measured data, which will be evaluated in this study. The kinetic parameters are taken from Meyer et al. (Meyer et al., 2020) and scaled with activity factors f_j according to the experimental results obtained at 556 K (see SI, Table S2). The equation further requires the stoichiometric coefficients $\nu_{i,j}$ and the catalyst mass m_{cat}. Furthermore, isothermal and isobaric conditions as well the absence of internal and external transport limitations are assumed, which was verified previously (Meyer et al., 2020). The model equations are axially discretized (50 nodes) with the method of lines and solved with the ode45 solver (explicit Runge-Kutta method) using default parameters in Matlab (Version R2017b).

Importantly, the signal at the reactor inlet is not ideal, due to the flow pattern in the piping between the 4/2-way valve and the reactor inlet. Therefore, we measured the step response at the reactor inlet ($x = 0$) by MS using Ar as tracer and applied polynomial fitting to derive the cumulative function of the RTD at the reactor inlet F_{fit} (results see SI, Figure S4). The measured step response was divided in three phases for simplification and according to the expected real laminar flow behavior (eq. (14)). It comprises an induction phase prior to t_1 and a steady-state beyond t_2. The transient phase between those boundaries is fitted. The values for $t_1 = 0.3\,\mathrm{s}$ and $t_2 = 8\,\mathrm{s}$ are defined ($F_{\mathrm{fit}}(t_1) = 0.01$, $F_{\mathrm{fit}}(t_2) = 0.99$) in order to neglect the influence of noise of the measured signal. This approach was used in order to calculate the molar flow rate at the reactor inlet $\dot{n}_i$ from the ideal step assumed for $\dot{n}_{i,\mathrm{in}}$ (eq. (15)).

$$F_{\mathrm{Ar},0}(t) = \begin{cases} 0 & t < t_1 \\ F_{\mathrm{fit}}(t) & t_1 \le t \le t_2 \\ 1 & t > t_2 \end{cases} \tag{14}$$

$$\dot{n}_i(x = 0, t) = F_{\mathrm{Ar},0}(t)\, \dot{n}_{i,\mathrm{in}} \tag{15}$$

3 Results and Discussion

This section is structured as follows. The results obtained for relevant reactants (CO and CO_2) and products (H_2O and CH_4) are presented in that order. For each component the build-up and back-

transient phase is reported consecutively. In order to avoid repetition the results are discussed in context of that sequence, as far as possible.

3.1 Build-up behavior of CO

Figure 1 (left) shows the step response for CO within the first 40 s of the build-up phase for CO feed containing compositions at different temperatures. Note, that the trend in CO for pure CO_2 methanation (z = 0) is not shown, as the amount of CO is close to the lower detection limit under the applied conditions, which is in accordance with literature (Gao et al., 2012; Koschany et al., 2016). After switching from a CO free to a CO rich feed an induction phase is observed within the first 5 s, which is caused by the RTD measured *in situ* and indicated by the dash-dotted line. In the following the CO step response increases approaching steady-state levels asymptotically. While the CO step response follows the RTD with small deviation for $z \geq 0.5$, the deviations observed for $z = 0.1$ will be discussed in the following.

Figure 1 (right) shows the transient molar flow rates, representing the difference between the expectations from RTD and the measured absolute molar flow rates. Negative values indicate a CO sink with respect to the gas phase, while positive values correspond to a source. Since adsorption of CO at the active surface and the conversion by chemical reaction are the only kinetic processes not covered by the RTD of the internal standard, CO is likely to be stored at the active surface by adsorption and converted by subsequent surface reactions. To make it more precise: We assume that the internal standard is chemically inert and capable of describing all kinetic processes related to pure transport of CO (e.g. pore diffusion), adequately. Therefore, any difference in RTD between the internal standard and CO can directly be associated to surface related processes, being the CO adsorption at the active surface and subsequent conversion the most important during the build-up phase. The simulated transient molar flow rates, depicted in grey, are obtained assuming steady-state reaction kinetics as introduced above. Therefore, adsorption processes of CO at the active surface are not covered by the simulation results.

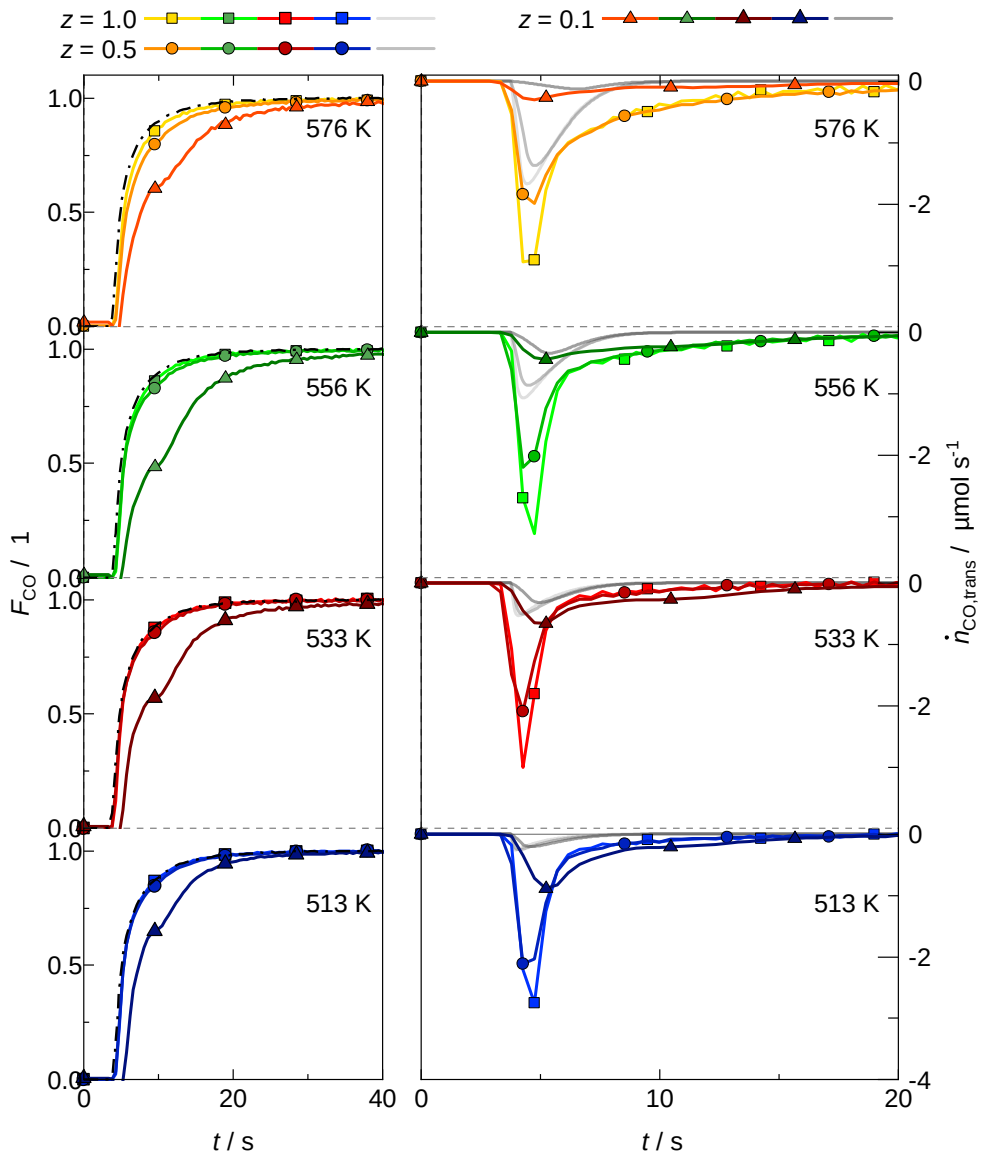

Figure 1: Left: Step response of CO (colored lines) and Ar (RTD, dash-dotted line); right: transient molar flow rates of CO for different CO_x feed ratios z and temperatures during the build-up phase; the simulated transient molar flow rates are shown in grey.

The measured transient molar flow rate first decreases more strongly than predicted by the simulation, which is equivalent with an increase in the stored amount of CO at the catalyst surface. Note, that the results of CO, only, allow no conclusion whether CO is adsorbed or if it is even converted. Following a minimum, the transient flow rate is approaching zero again and thus steady-state. The minimum is more pronounced than simulated and shows that the driving force for CO adsorption at the catalyst surface is high in the early stage of the build-up phase, where the surface coverage by CO is still low. With increasing CO surface coverage, the adsorption rate decreases and thus the transient molar flow rate approaches zero, indicating that the CO surface coverage is in steady-state. Furthermore,

significant deviations with respect to the temperature dependency are observed. Obviously, the simulated transient molar flow rates of CO predict a sink being more pronounced at higher temperatures. This trend is reasonable, since the hydrogenation rate of CO increases with temperature. In contrast, adsorption is favored at lower temperatures, which compensates decreasing reaction rates to a certain extent, leading to the small effective impact of temperature on the measured transient molar flow rates.

Figure 1 (right) also shows that the absolute value of the minimum transient molar flow rate is rather constant in the investigated temperature range, while a clear trend can be observed related to the z values. In particular, the minimum is expressed more significantly for higher CO fractions in the feed gas and the integrated transient molar flow rate over time increases with the CO fraction, as well. The significant effect of the CO concentration on CO adsorption and the absence of a temperature effect agrees with literature (Polizzotti and Schwarz, 1982; Biloen et al., 1983; Alstrup, 1995). For example, Polizotti et al. (Polizzotti and Schwarz, 1982) stated that the catalyst surface remains nearly saturated with CO irrespective of the temperature in the range between 500 and 700 K. In contrast the amount of adsorbed CO depends clearly on its partial pressure (Bartholomew and Pannell, 1980), which leads to a decrease of the surface coverage of CO with decreasing CO partial pressure. The results also correspond to our findings for simultaneous CO_x methanation under steady-state conditions exhibiting exclusive CO hydrogenation for $z > 0.1$, even though CO_2 is present (Meyer et al., 2020). Under those conditions, CO occupies essentially all sorption sites, which effectively prevents CO_2 from adsorption (Meyer et al., 2020).

3.2 Back-transient behavior of CO

Figure 2 shows the results obtained during the back-transient phase of CO after switching from CO rich to CO free feed gas. The step response is provided in the SI (Figure S5) and show no significant difference to the RTD irrespective of feed gas compositions and temperatures. Based on the transient molar flow rates, however, a dependence on temperature and CO_x ratio can be observed. At first the transient molar flow rate is positive, indicating CO desorption from the surface into the gas phase. In

the following, the transient molar flow rate drops for all CO containing feeds to negative values before approaching zero in the steady-state. The negative transient molar flow rates suggest that CO from the gas phase adsorbs again at sorption sites just released by conversion into CH_4. Therefore, the desorption step appears to be consecutively followed by re-adsorption and subsequent conversion during the back-transient phase.

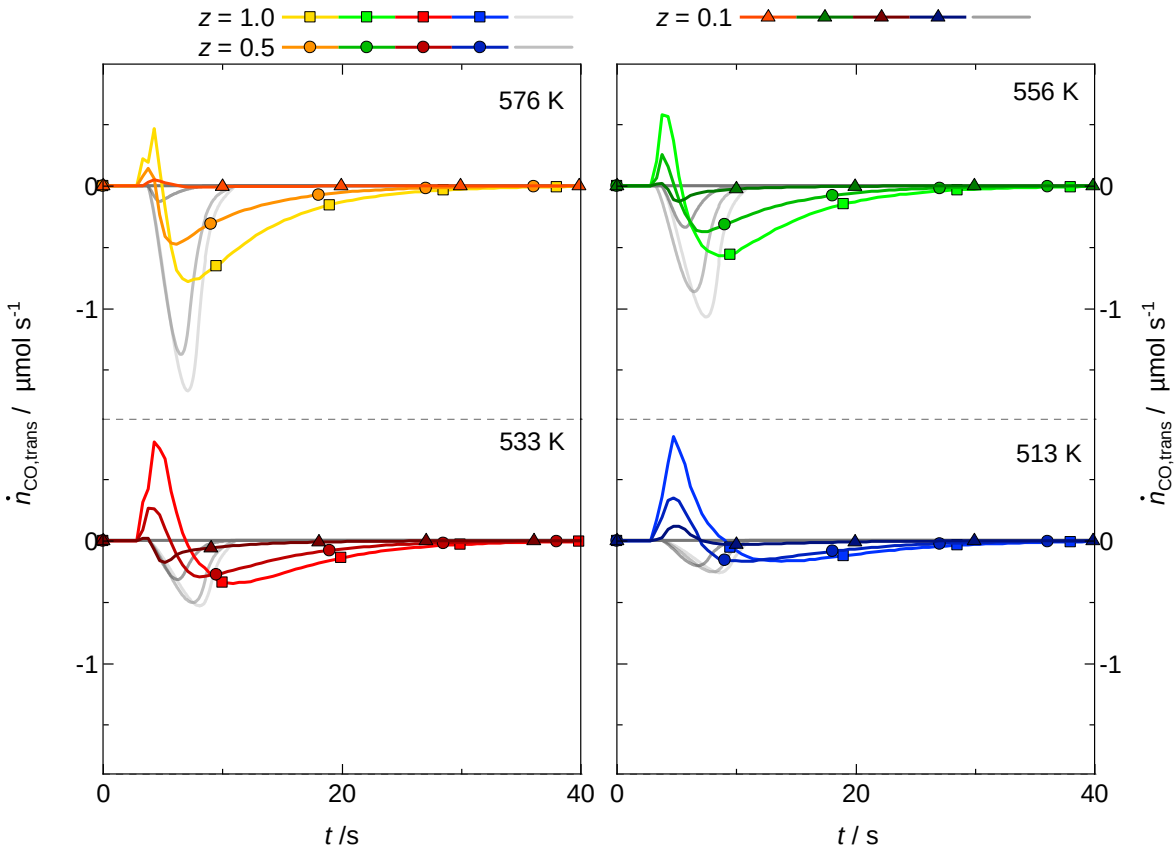

Figure 2: Transient molar flow rates of CO for different CO_x feed ratios z and temperatures during the back-transient phase; the simulated transient molar flow rates are shown in grey.

Furthermore, a significant effect of the CO_x feed ratio and the temperature is apparent from the measured as well as the simulated transient molar flow rates both agreeing with each other with respect to the trends. For a decreasing CO content in the feed gas mixture the transient molar flow rate diminishes, since the reservoir of adsorbed CO becomes smaller, and the reported effects are thus less expressed. The decrease in temperature, interestingly, affects the intensity of the desorption and re-adsorption step. This becomes apparent by comparing the integrated values of the transient molar flow rate distinguished between the desorption (positive values) and re-adsorption (negative values) phase (Table 3). For $z \geq 0.5$ the desorbed molar amount of CO decreases with increasing temperature,

while the re-adsorbed amount increases. This can be explained by the increasing reaction rate with temperature, which leads to fast conversion of adsorbed CO species and therefore more available sorption sites during the transient phase. Consequently, desorption is less likely, while re-adsorption is favored. For $z = 0$ no clear trend can be observed, since quantification is difficult regarding the precision of measurement. These findings are supported by literature, as Underwood et al. have shown for pure CO methanation that a small amount of CO desorbs, indeed (Underwood and Bennett, 1984). Furthermore, this might also indicate that CO adsorbs at the catalyst surface without being transformed into a reactive carbon species at lower temperatures, which is in accordance to Agnelli et al. (Agnelli et al., 1998). The re-adsorption during the back-transient phase, however, is not yet reported in scientific literature to the best of our knowledge.

Table 3: Total molar amount of CO desorbed ($n_{\mathrm{trans},+}$) and re-adsorbed ($n_{\mathrm{trans},-}$) during the back-transient phase obtained by integration over the respective time interval.

	molar amount of CO / µmol							
	576 K		556 K		533 K		513 K	
z / 1	$n_{\mathrm{trans},+}$	$n_{\mathrm{trans},-}$	$n_{\mathrm{trans},+}$	$n_{\mathrm{trans},-}$	$n_{\mathrm{trans},+}$	$n_{\mathrm{trans},-}$	$n_{\mathrm{trans},+}$	$n_{\mathrm{trans},-}$
1.0	0.5	7.2	0.8	5.8	1.7	4.1	2.2	2.2
0.5	0.1	3.7	0.2	3.3	0.4	2.9	0.8	2.0
0.1	0.0	0.0	0	0.5	0	0.8	0.2	0.3

3.3 Build-up behavior of CO_2

Figure 3 shows the transient molar flow rates for CO_2 with the corresponding step response provided in the SI (Figure S6). The deviation of the observed step response of CO_2 from the RTD for pure CO methanation conditions ($z = 1$) indicates that the formation of CO_2 is the result of a slow secondary reaction path. This is supported by Zarfl et al. (Zarfl et al., 2015), where the Boudouard and/or the WGS reaction are denoted as the most likely reaction pathways (Kopyscinski et al., 2010; Gao et al., 2012). The transient molar flow rates are close to zero, though, since the CO_2 formation under steady-state conditions is negligible (see SI, Table S1).

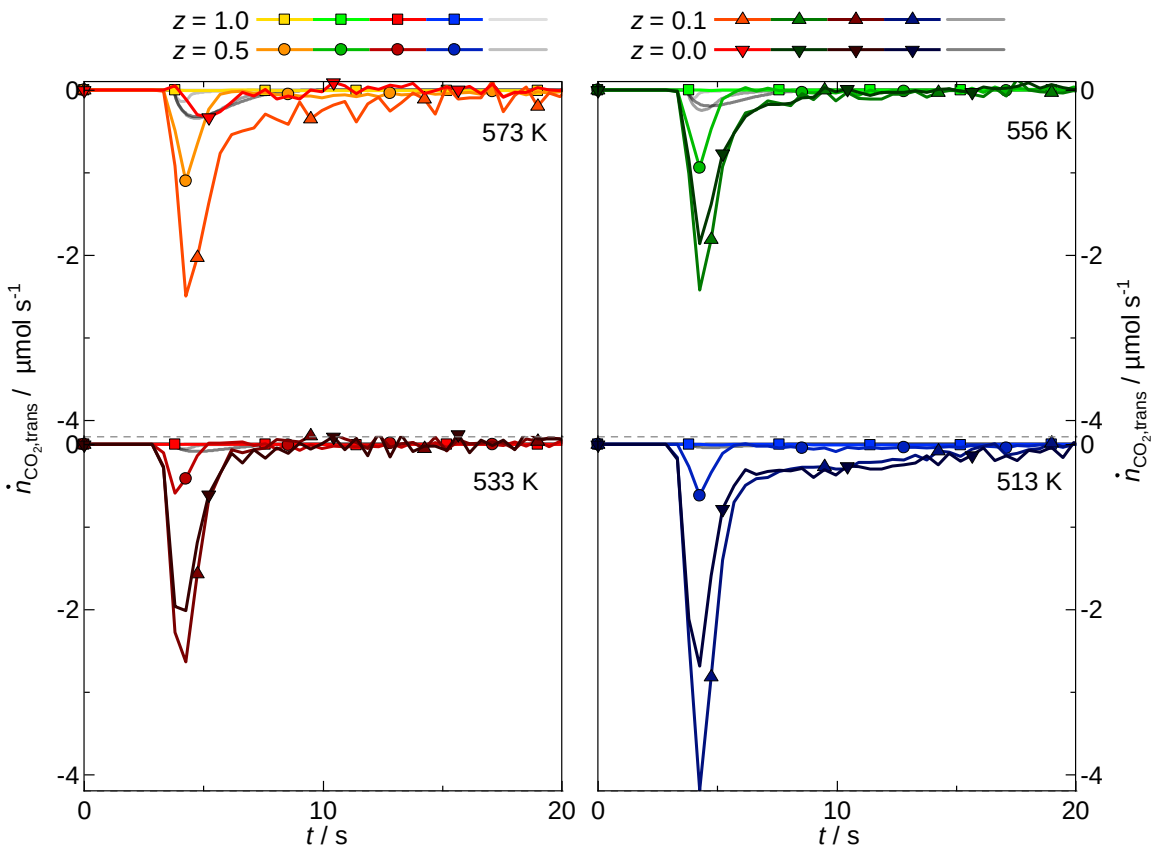

Figure 3: Transient molar flow rates of CO_2 for different CO_x feed ratios z and temperatures during the build-up phase; the simulated transient molar flow rates are shown in grey.

The negative transient molar flow rates indicate interaction of CO_2 with the solid surface similar to CO, exhibiting the minimum early during the build-up phase, as well. The amount of adsorbed CO_2, expressed by the minimum and the integrated transient molar flow rate, is reduced by increasing the fraction of CO in the feed (raising z). For an equimolar mixture of CO and CO_2, for instance, only a small minimum is observed, which suggests a mainly inert behavior of CO_2 at high CO concentrations. This agrees with several studies performed under steady-state conditions (Van Herwijnen, 1973; Polizzotti and Schwarz, 1982; Weatherbee and Bartholomew, 1982; Biloen et al., 1983; Alstrup, 1995; Falbo et al., 2019; Meyer et al., 2020). In particular, CO adsorption is favored compared to the other species, which is even more pronounced at high CO concentrations. Therefore, CO occupies nearly all sorption sites, preventing CO_2 from adsorption, which consequently acts rather inert also with respect to the hydrogenation reaction. The negative transient molar flow rate at $z = 0.5$, however, might be caused by non-competing adsorption of CO_2 on the support being Al_2O_3 in the present study (Friedland et al., 2020). While Al_2O_3 is known for its potential to chemisorb CO_2 (Manchado et al., 1994), the adsorption

potential of CO is low (Manchado et al., 1994) and thus assumed negligible. The deviation between measured and simulated transient molar flow rates confirms that CO_2 indeed adsorbs on the surface.

3.4 Back-transient behavior of CO_2

The step response (Figure 4, left) show no significant deviation of the CO_2 back-transient behavior from the RTD except for pure CO hydrogenation ($z = 1$). Based on the evaluation of the transient molar flow rates, however, an interaction with the catalyst surface is evident for $z < 1$ (Figure 4, right). Similar to CO, a positive transient molar flow rate of CO_2 is observed during the early stage, indicating desorption of previously adsorbed CO_2 into the gas phase. The amount of desorbed CO_2 is decreasing strongly with raising temperature (Table 4), which is probably weakly bound on the surface (Falconer and Zağli, 1980; Friedland et al., 2020). In the following, the transient molar flow rate drops as more CO_2 is converted, which agrees with the simulated values at higher temperatures regarding the principle trend. The quantitative deviation between the measured and simulated transient molar flow rates is caused by the sorption processes, not accounted for in the steady-state reaction kinetics. At high temperatures the transient molar flow rate even reaches negative values, which indicates re-adsorption of CO_2 in the back-transient phase similar to the respective discussion for CO. In contrast to the steady-state results conversion of CO_2 can be detected even for high amounts of CO in the feed gas mixture (e.g. $z = 0.5$) (Meyer et al., 2020). This can be explained by the simultaneous decrease of CO and CO_2 in the gas phase during the back-transient half-period. Therefore, the dominating CO adsorption at the surface becomes less pronounced over time, which provides more sorption sites available for CO_2 to adsorb and subsequently to be converted to CH_4.

In the case of pure CO methanation ($z = 1$) the CO_2 step response exhibits a peak, whose temporal occurrence and maximum is temperature sensitive. Note, that the trends are displayed in the normalized form and that the corresponding absolute amount of produced CO_2 is small. Nevertheless, this peak most likely results from a reaction process or desorption from the support, as the CO_2 gas phase concentration is low and thus CO_2 should desorb instantaneously after formation under given conditions (Falconer and Zağli, 1980; Friedland et al., 2020).We assume that a particular reaction

mechanism is responsible for this observation, where oxygen containing species stored at the catalyst surface are converted. It has to be stated, however, that further experiments are required to fully understand the underlying reaction mechanism to this observation. Even though, such behavior for CO_2 under unsteady-state CO methanation conditions is not yet reported, Mutz et al. (Mutz et al., 2017) suggest different possible oxygen sources. In particular, CO_2 could either be generated by a reaction intermediate containing oxygen, the WGS reaction, or directly from the catalyst (e.g. from the lattice).

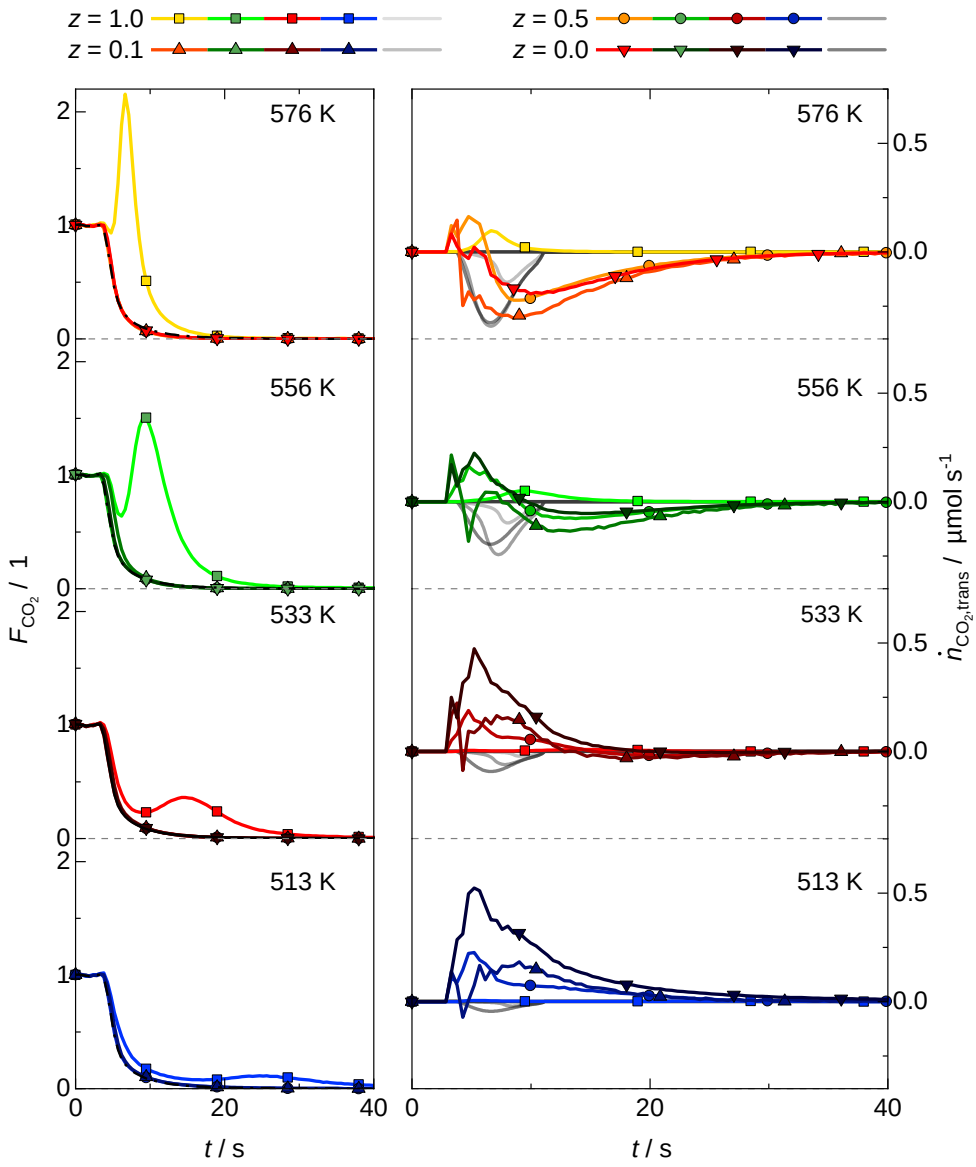

Figure 4: Left: Step response of CO_2 (colored lines) and Ar (RTD, dash-dotted line); right: transient molar flow rates of CO_2 for different CO_x feed ratios z and temperatures during the back-transient phase; the simulated transient molar flow rates are shown in grey.

Table 4: Total molar amount of CO_2 desorbed ($n_{\mathrm{trans},+}$) and re-adsorbed ($n_{\mathrm{trans},-}$) during back-transient phase obtained by integration over the respective time interval.

	molar amount of CO_2 / µmol							
	576 K		556 K		533 K		513 K	
z / 1	$n_{\mathrm{trans},+}$	$n_{\mathrm{trans},-}$	$n_{\mathrm{trans},+}$	$n_{\mathrm{trans},-}$	$n_{\mathrm{trans},+}$	$n_{\mathrm{trans},-}$	$n_{\mathrm{trans},+}$	$n_{\mathrm{trans},-}$
1.0	0.3	0.0	0.3	0.0	0.1	0.0	0.0	0.0
0.5	0.4	2.3	0.5	1.0	0.8	0.2	1.6	0.0
0.1	0.1	3.9	0.2	1.7	0.7	0.4	1.8	0.0
0.0	0.0	2.4	0.7	0.7	2.5	0.1	4.3	0.0

3.5 Build-up behavior of H_2O

In contrast to the previously discussed reactants CO and CO_2 the product H_2O is formed stoichiometrically by chemical reaction as an adsorbed species, which subsequently desorbs into the gas phase (Miao et al., 2016). The transient molar flow rates of H_2O during the build-up phase show negative values during the complete half-period (Figure 5) corresponding to a temporal delay from the RTD (see step response in SI, Figure S7), which is most pronounced for low temperature and high CO content in the feed gas. Moreover, the measured transient molar flow rates are negative for all investigated conditions, whereas the simulated results exhibit positive values. This fundamental deviation can be explained by the storage of H_2O at the catalyst surface, especially by adsorption at Al_2O_3 sites (Morimoto et al., 1971), which buffers the H_2O response and is not considered in the model. Furthermore, the surface adsorption can also explain that the strongest temporal delay in the transient molar flow rates is observed for pure CO methanation ($z = 1$), since the H_2O production rate is decreasing with increasing CO fraction in the feed, due to stoichiometric reasons. Hence, more time is required to fill the H_2O storage capacity for smaller H_2O formation rates and therefore for increasing values of z. Since the sorption capacity decreases and the H_2O formation rate increases with raising temperature, H_2O appears earlier in the gas phase and therefore the deviation from RTD becomes smaller. Our results, however, seem to contradict earlier studies by Klusáček and Stuchlý (Klusáček and Stuchlý, 1995) and Fujita et al. (Fujita et al., 1987), where a rapid overshoot in the H_2O response is

reported. We attribute those observations to the lower storage capacity of H_2O for the catalysts used: Klusáček and Stuchlý (Klusáček and Stuchlý, 1995) used Ni/SiO_2, while Fujita et al. (Fujita et al., 1987) pure Ni for their experiments. In particular, it is well-known that the sorption capacity of H_2O at SiO_2 surfaces is significantly smaller than at Al_2O_3 (Morimoto et al., 1971), which therefore renders the observed discrepancies between our results and literature to be plausible.

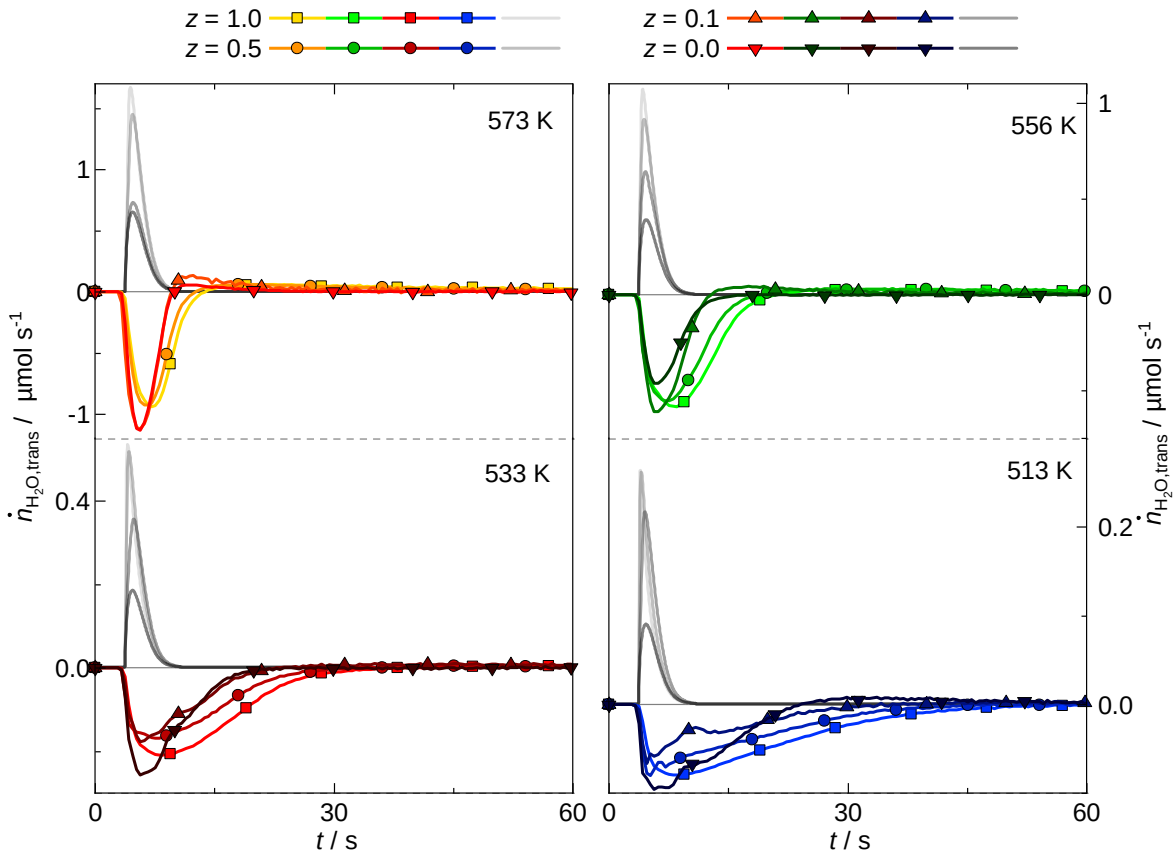

Figure 5: Transient molar flow rates of H_2O for different CO_x feed ratios z and temperatures during the build-up phase; the simulated transient molar flow rates are shown in grey

3.6 Back-transient behavior of H_2O

Figure 6 shows the back-transient behavior of H_2O, which exhibits positive transient molar flow rates throughout the half-period for both the experimental and simulation results (for step response see SI, Figure S8). This can be explained by the decreasing CO_x fraction in the gas phase during the back-transient phase and thus the increasing H_2/CO_x ratio with time. Therefore, the H_2/CO_x ratio passes kinetically favored values for the CH_4 and H_2O formation, which causes the positive transient molar flow rates (Meyer et al., 2020). The simulated profiles exhibit a narrow distribution in the early stage of the back-transient phase, while the measured values also show significant amounts of H_2O

appearing in the gas phase in a later stage. The steady-state kinetics used for the simulations account for competitive adsorption of the involved species and the implications on the reaction rate, assuming steady-state, though. Hence, the simulated transient molar flow rates exhibit an increasing H_2O release with increasing z values, since the positive effect of high H_2/CO_x ratios is most pronounced for those cases (Meyer et al., 2020). The tailing in the H_2O signal in the later stage, therefore, is most likely caused by slow desorption of H_2O stored at the alumina surface, which is not included in the model. Alternatively, hydrogenation of intermediate formate species (COOH) present at the catalyst surface, which are postulated in literature to be present with a significant amount at the surface under steady- and unsteady-state CO and CO_2 methanation conditions (Fujita et al., 1991; Marwood et al., 1994; Falbo et al., 2019; Burger et al., 2020), could cause formation and desorption of H_2O and thereby effect the later stage of the back-transient behavior. The profiles for all CO_x feed gas mixtures become similar asymptotically, indicating that it is determined by the same physical processes.

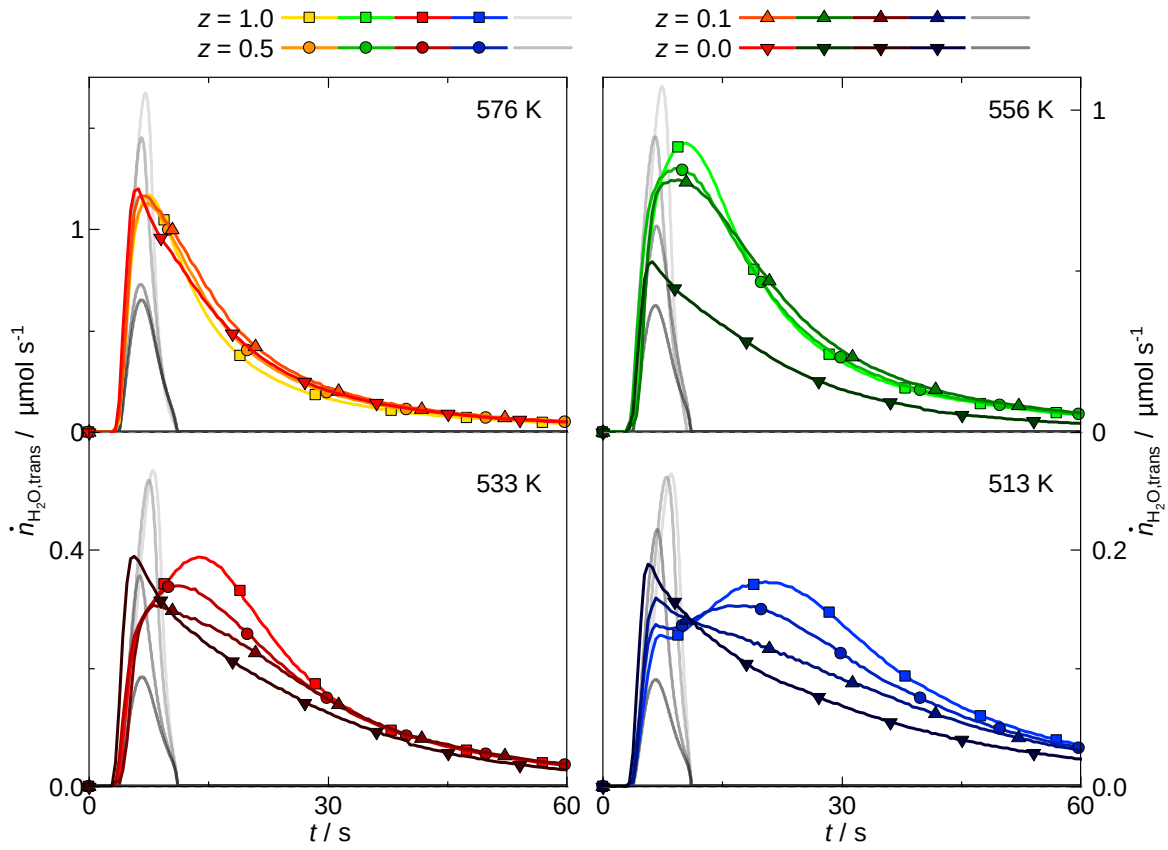

Figure 6: Transient molar flow rates of H_2O for different CO_x feed ratios z and temperatures during the back-transient phase; the simulated transient molar flow rates are shown in grey.

While the measured profiles are almost identical for all CO_x ratios at 576 K, a deviation develops at lower temperatures. For the case of pure CO_2 ($z = 0$) the transient molar flow rate exhibits a maximum in the early stage followed by an exponential decay, indicating that the desorption of H_2O is the only relevant process. For CO containing feed gas mixtures, though, a maximum is visible in a later stage of the back-transient phase, which is prominent for 513 K and pure CO methanation ($z = 1$). This maximum shifts backwards in time with increasing temperature and finally coincides with the maximum for pure CO_2 methanation at 576 K. The temperature induced temporal shift of the maximum for CO methanation ($z = 1$) suggests that a thermally activated reactive process leads to the occurrence of H_2O in the gas phase. The observation of two different maxima also indicates that two different processes are responsible for the H_2O back-transient behavior in case of CO containing feed gas mixtures, whereas for pure CO_2 methanation only one process seems to be responsible. In particular, we assume that H_2O desorption from the solid surface is occurring irrespective from the CO_x ratio, while intermediate species adsorbed at the surface are only formed at higher CO partial pressures. This is plausible, since the formation of H_2O and its adsorption depends on methanation stoichiometry and surface chemistry of the solids only, but is independent on the CO content in the gas phase. The presence and type of intermediate surface species, however, strongly depend on the reaction mechanism governed by the partial pressures of CO, CO_2 and H_2 (Fujita et al., 1993; Miao et al., 2016).

3.7 Build-up behavior of CH_4

The step response of CH_4 in the build-up phase exhibits an overshoot in the CH_4 signal and higher values than predicted from pure RTD (Figure 7). These observations are in particular depending on temperature, while the trend is similar for all z values. The corresponding measured transient molar flow rates are negative initially but turn to positive values during the build-up phase. The negative values indicate a delayed release of CH_4 compared to the RTD, due to the kinetics of the consecutive formation and desorption steps, while positive values indicate an accelerated CH_4 release into the gas phase. The simulated transient molar flow rates are always positive and immediately appear according

to the RTD. Similar to the discussion for the H_2O signal in the back-transient phase the positive values can be explained by the passing of kinetically favored H_2/CO_x ratios during the build-up. The measured profiles also exhibit positive transient molar flow rates, since the catalyst surface is initially saturated by H_2, due to the previous back-transient phase under H_2/He flow. This favors the CH_4 formation kinetically, as well. In addition, the dynamics of competitive adsorption of the involved species and their impact on the reaction kinetics have to be considered. In particular, CO is capable of displacing H_2 from the surface, which leads to a reduction of the methanation rate for high CO partial pressures (Underwood and Bennett, 1984; Bundhoo et al., 2009). Other studies emphasize the inhibiting effect of CO on the CH_4 methanation, as well (Goodman et al., 1980; Stuchlý and Klusáček, 1993; Aparicio, 1997). Since, the observed overshoot is smaller and delayed compared to the simulated one, it is most probably caused by passing through an optimal ratio of the adsorbed species, during the transient change of the gas phase composition.

It has to be mentioned that the sequence of the measured maximum transient molar flow rate changes with respect to CO_x ratio over the temperature range. At high temperatures the observed maximum is higher with increasing CO content in the feed gas mixture, while the opposite holds for lower temperatures. According to literature a change in the kinetic regime at temperatures of ca. 490 to 510 K might be responsible for this observation (Goodman et al., 1980; Polizzotti and Schwarz, 1982; Friedland, 2018). Goodman et al. (Goodman et al., 1980) show in their study that at temperatures around 500 K the reaction rate is nearly independent on the pressure, whereas at higher temperatures a clear pressure dependency can be seen. They concluded that at higher temperatures the amount of carbon at the catalyst surface can be decreased by an increasing H_2 partial pressure, which is not possible at lower temperatures where CO is strongly adsorbed (Agnelli et al., 1998). Furthermore, increasing the CO_2 content in the feed gas composition reduces the overshoot in the CH_4 production during the build-up phase due to the decreasing inhibition by CO, which is also predicted by the steady-state model. Aparicio observed the same effect for the variation of the CO partial pressure for the pure CO methanation (Aparicio, 1997), stating that with a decrease of CO in the gas phase the CO coverage

cannot longer approach unity, which dampens the inhibiting effect. In contrast to our results, they observed the opposite temperature induced effect, as the overshoot in CH_4 weakens with increasing temperature. However, they conducted their study with a large excess of H_2, which might explain the difference, as our results are in accordance with Bundhoo et al. (Bundhoo et al., 2009) and Stuchlý and Klusáček (Stuchlý and Klusáček, 1993).

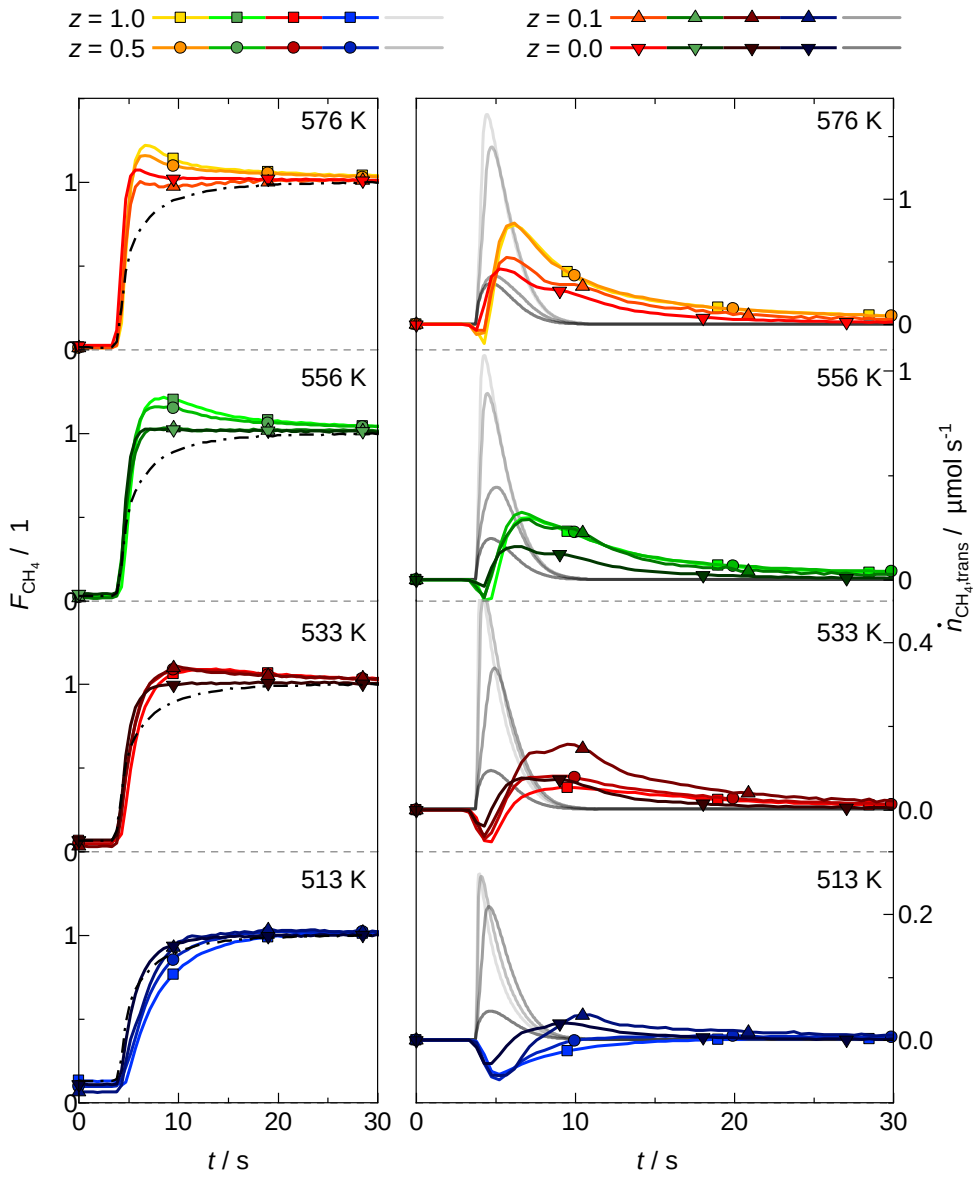

Figure 7: Left: Step response of CH_4 (colored lines) and Ar (RTD, dash-dotted line); right: transient molar flow rates of CH_4 for different CO_x feed ratios z and temperatures during the build-up phase; the simulated transient molar flow rates are shown in grey.

Interestingly, the temporal occurrence of the maximum in the transient molar flow rate of CH_4 nearly coincides with the minimum in H_2O, as Figure 8 shows exemplarily for different temperatures and $z =$

0.1. Since both CH_4 and H_2O are formed stoichiometrically, this observation suggests that H_2O is adsorbed at the surface, while CH_4 desorbs almost immediately after being formed. Hence, the presence of adsorbed H_2O species does not hamper the CH_4 formation drastically, while H_2O in the gas phase is reported to inhibit the CH_4 formation rate (Marwood et al., 1994; Borgschulte et al., 2013). It has to be mentioned that the observation strongly depends on the catalyst support used, since Al_2O_3 provides a significant sorption capacity for H_2O in contrast to SiO_2. Klusáček and Stuchlý (Klusáček and Stuchlý, 1995) as well as Fujita et al. (Fujita et al., 1987), for instance, report a slow increase in the CH_4 and a fast increase in the H_2O signal. Both studies used either SiO_2 as support material (Klusáček and Stuchlý, 1995) or pure Ni (Fujita et al., 1987), both known to provide a lower storage capacity for H_2O compared to Al_2O_3 used in the present work.

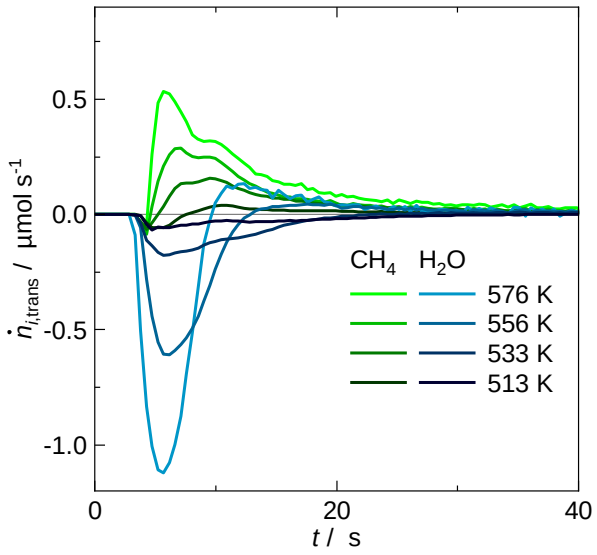

Figure 8: CH_4 and H_2O transient molar flow rates for $z = 0.1$ at different temperatures during build-up phase.

3.8 Back-transient behavior of CH_4

Figure 9 (left) shows that a switch from a CO_x rich to a CO_x free feed gas is accompanied with a positive deviation of the CH_4 step response compared to the RTD with a distinct maximum for CO containing feed gas mixtures. The maximum increases with decreasing temperature by a factor of up to 3.5 with respect to the steady-state value. This indicates the high sensitivity of the system towards an exchange of CO_x rich with a CO_x free feed especially for low temperatures and high z values and agrees with

literature (Bundhoo et al., 2009). Furthermore, the maximum decreases with decreasing z and is not observed for $z = 0$ as expected for pure CO_2 methanation conditions (Van Ho, 1980; Fujita et al., 1991; Marwood et al., 1994).

The corresponding transient molar flow rate is positive throughout the complete back-transient phase (Figure 9, right). The duration of the process as well as the total amount of released CH_4 thereby depends strongly on temperature and CO_x feed ratio (Table 5). At higher temperatures, the process is completed faster and more CH_4 is produced, while higher z values also lead to higher amounts of released CH_4. In all cases the amount of released CH_4 predicted by simulation is significantly lower than the measured values, while the predicted duration of CH_4 appearance is shorter and independent on temperature. This indicates that additional carbonaceous species are stored at the catalyst surface during the dynamic experiments, which are converted into CH_4 under transient conditions and thereby increase the CH_4 signal above the values predicted from steady-state kinetics. In contrast to pure CO_2 feed gas mixtures for CO containing feeds ($z > 0$) the form of the CH_4 transient molar flow rate changes with temperature. At 576 K the CH_4 profile exhibits one maximum and an exponential decay, whereas with decreasing temperature the peak broadens and a shoulder appears for high fractions of CO ($z \geq 0.5$). This indicates that two species at the catalyst surface are hydrogenated to CH_4 under CO_x methanation conditions, whereas only one seems to be converted in case of pure CO_2 methanation. The first species is immediately converted leading to the appearance of the early maximum, which occurs at ca. 7 s for all cases. The temporal occurrence of this first maximum is predicted correctly by the simulations assuming steady-state kinetics. This underlines that the highly reactive intermediate is hydrogenated immediately without preceding dynamic effects at the catalyst surface, which are neglected by the model. The hydrogenation of the second species is temperature dependent and appears as the shoulder following the maximum in particular at 513 K. Similar to the discussion of the back-transient phase for H_2O the second maximum, pronounced as a shoulder here, shifts to earlier times with increasing temperature and finally coincides with the first maximum.

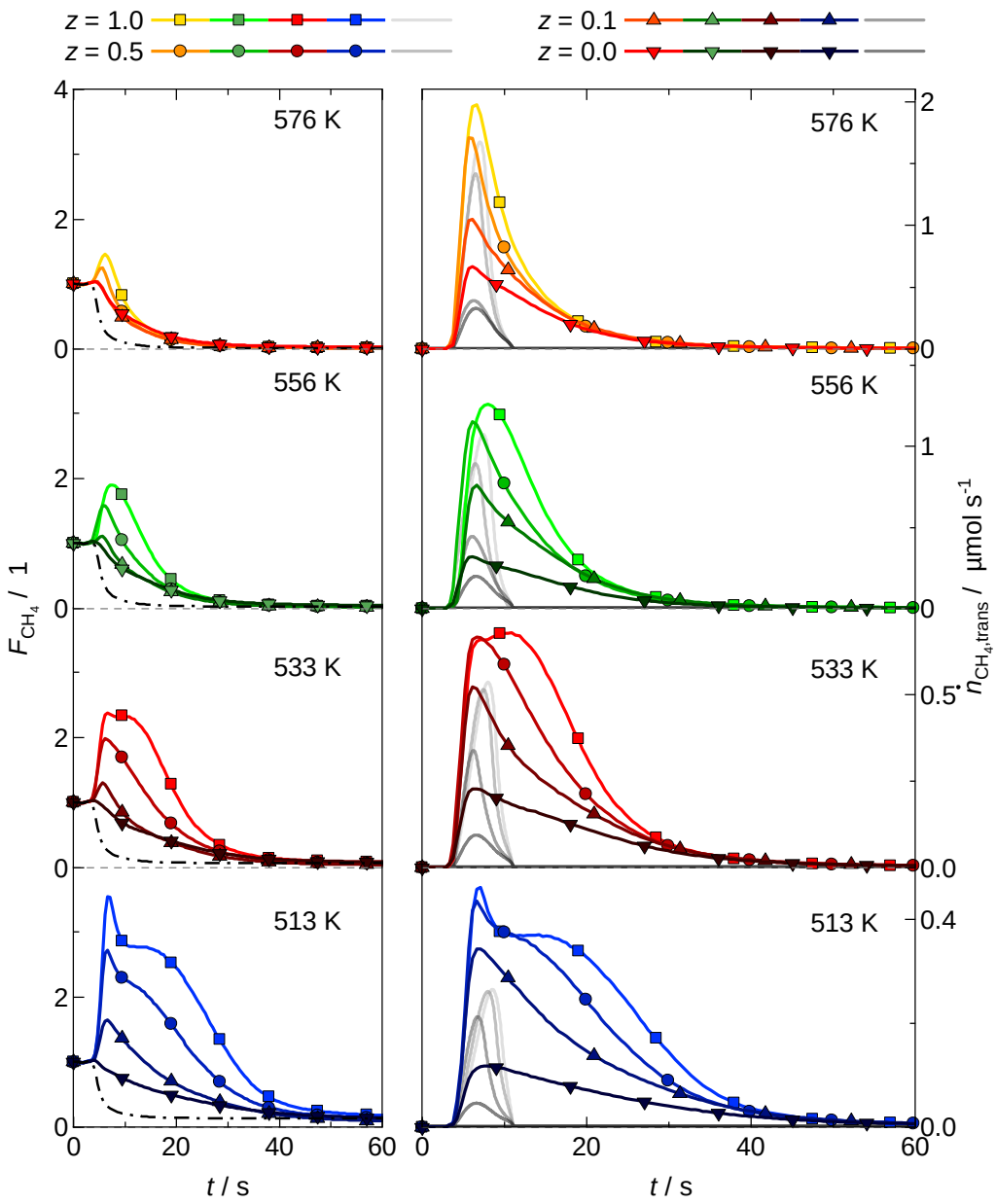

Figure 9: Left: Step response of CH_4 (colored lines) and Ar (RTD, dash-dotted line); right: transient molar flow rates of CH_4 for different CO_x feed ratios z and temperatures during the back-transient phase; the simulated transient molar flow rates are shown in grey.

The presence of highly reactive intermediates adsorbed at the surface is supported by literature reports, which suggest that a solely carbon containing species, denoted as C_α, under steady-state (Gałuszka et al; Alstrup, 1995; Sehested et al., 2005) and unsteady-state (Underwood and Bennett, 1984; Efstathiou and Bennett, 1989; Fujita et al., 1991; Fujita et al., 1993; Fujita and Takezawa, 1997) methanation conditions exists. Fujita et al. (Fujita et al., 1993) conducted DRIFTS measurements for transient CO and CO_2 hydrogenation experiments and show that the highly reactive species is not present under CO_2 methanation conditions, which is consistent with our results. The authors observed

mainly bridged adsorbed CO along with a formate species at the catalyst surface during the CO_2 hydrogenation, whereas a considerable amount of linear adsorbed CO and C_α exists for CO methanation. It is concluded that the linear adsorbed CO retards the hydrogenation of C_α, but disappears rapidly after switching to pure H_2, which allows a fast hydrogenation of C_α, subsequently. According to Yadav and Rinker (Yadav and Rinker, 1992) the amount of atomic carbon stored at the surface increases with increasing CO/H_2 molar ratio, which is consistent with our results, since the maximum in CH_4 signal is reduced for low z values and thus low CO/H_2 ratios. The chemical nature of the reactive species, however, being pure carbon or not, is still under debate. Recent studies proposed kinetic rate equations for CO_2 and even CO_x methanation via hydrogen assisted C-O bond cleavage steps towards COH intermediates (Underwood and Bennett, 1984; Koschany et al., 2016; Falbo et al., 2019; Burger et al., 2020), whereas Burger et al. (Burger et al., 2020) found no evidence of elemental carbon species even under CO methanation conditions. Importantly, the re-adsorption of CO and CO_2 observed in the back-transient phase most probably also contribute to the formation of excess CH_4 in addition to the carbonaceous species adsorbed at the catalyst surface. This was often neglected in the past (Van Ho, 1980; Underwood and Bennett, 1984; Yadav and Rinker, 1992; Fujita et al., 1993; Stuchlý and Klusáček, 1993), probably because re-adsorption was not observed so far, due to experimental limitations.

Table 5: Total molar amount of CH_4 desorbed ($n_{\mathrm{trans},+}$) during back-transient phase obtained by integration over the respective time interval.

	molar amount of CH_4 / µmol			
	576 K	556 K	533 K	513 K
z / 1	$n_{\mathrm{trans},+}$	$n_{\mathrm{trans},+}$	$n_{\mathrm{trans},+}$	$n_{\mathrm{trans},+}$
1.0	15.0	13.8	11.0	9.0
0.5	12.9	11.4	9.0	7.6
0.1	10.3	8.7	6.6	5.6
0.0	7.5	4.4	3.9	2.5

4 Conclusion

The influence of CO, CO_2 and mixtures thereof on the transient behavior of the reactants during methanation was investigated experimentally for a Ni/Al_2O_3 catalyst in a continuously operated fixed-bed reactor under technical relevant conditions by means of the novel PTK method. Therefore, periodic step changes are performed at the reactor inlet between CO_x rich and CO_x free gas compositions and vice versa, in order to study the build-up and back-transient half-period. For all reactants the temporal profiles of the periodic step response are obtained and deconvoluted from the RTD measured *in situ*. Moreover, an unsteady-state reactor model is developed based on steady-state CO_x methanation kinetics. This sophisticated approach combining experiments and simulations was used to deduce the transient behavior of the kinetic processes taking place at the solid catalyst surface and their impact on the observed unsteady-state reactor behavior. From the obtained results the following conclusions can be drawn:

1. A reactor model based on unsteady-state material balances and steady-state reaction kinetics is not capable to predict the transient behavior of the reactor, neither during the build-up nor in the back-transient phase. The kinetic processes taking place at the catalyst surface are strongly affecting the reactor response, instead, and need to be considered at least for step changes at the reactor inlet. In addition, the storage capacities of the species by adsorption at the solid surface play an important role for the reactor response.
2. The experimental results obtained for CO, CO_2, CH_4 and H_2O during build-up and back-transient phase are consistent and agree with literature reports in principle. In particular, the support provides significant storage capacity for adsorbed H_2O and CO is found to strongly adsorb at the active material and thereby inhibits CO_2 hydrogenation. In addition to the state-of-knowledge, CO and CO_2 are found to re-adsorb at the catalyst surface during the back-transient phase and are partially converted into CH_4 and H_2O.
3. The dynamic reactor behavior is strongly influenced by the kinetic processes occurring at the solid surface, which are governed by the CO_x and the H_2/CO_x ratio, as well as the reaction temperature.

In particular, maxima in the transient signal of CH_4 compared to the steady-state values are observed during both the build-up and back-transient phase, induced by passing kinetically favored gas compositions for the CH_4 and H_2O formation. Furthermore, two adsorbed intermediate species with different reactivity are postulated for CO containing feeds, while only one is present for CO_2 methanation.

Hence, the results obtained via the PTK method provide the experimental basis to identify, parameterize and validate the surface reaction steps being significant for an appropriate transient kinetic model. The present work focuses on the impact of the CO/CO_2 ratio at a constant CO_x/H_2 ratio on the transient response, in order to demonstrate the capabilities of the PTK method to elucidate mechanistic aspects. For deeper investigation of the dynamic processes on the catalyst surface, however, the variation of the CO_x/H_2 ratio and the pressure is necessary, as well.

The reported results are based on observations at the macroscopic level by analyzing the transient molar flow rates at the reactor outlet. Therefore, complementary *in situ* or *operando* measurements with emphasis on the dynamics of processes at the solid surfaces are required for a full kinetic understanding of the dynamic reactor behavior, which are matter of ongoing research. This knowledge provides the basis to derive reaction kinetics valid under unsteady-state conditions mandatory to predict the behavior of methanation reactors in PtG application scenarios. In particular, a micro-kinetic model is recommended, which also considers the storage capacity of the reactants at the active material and support. The model improved by appropriate micro-kinetics also allows the design of suitable reactors offering sufficient tolerance towards fluctuating feed gas compositions. In principle, the reported methodology can also be applied to other heterogeneously catalyzed reactions directly, e.g. ammonia or methanol synthesis, also relevant for chemical storage of renewable energy.

Acknowledgment

The authors want to thank Sasol Germany GmbH for providing the support material. Henning Becker is acknowledged for the very valuable scientific discussion.

Funding

This research did not receive any specific grant from funding agencies in the public, commercial, or not-for-profit sectors.

5 References

Adesina, A.A., Hudgins, R.R., Silveston, P.L., 1995. Fischer-Tropsch synthesis under periodic operation. Catal. Today 25 (2), 127–144. 10.1016/0920-5861(95)00103-M.

Agnelli, M., Swaan, H.M., Marquez-Alvarez, C., Martin, G.A., Mirodatos, C., 1998. CO hydrogenation on a nickel catalyst: II. A mechanistic study by transient kinetics and infrared spectroscopy. J. Catal. 175 (1), 117–128. 10.1006/jcat.1998.1978.

Alstrup, I., 1995. On the kinetics of CO methanation on nickel surfaces. J. Catal. 151 (1), 216–225. 10.1006/jcat.1995.1023.

Aparicio, L.M., 1997. Transient Isotopic Studies and Microkinetic Modeling of Methane Reforming over Nickel Catalysts. J. Catal. 165 (2), 262–274. 10.1006/jcat.1997.1468.

Bailey, J.E., Horn, F.J.M., Lin, R.C., 1971. Cyclic operation of reaction systems: Effects of heat and mass transfer resistance. AIChE J. 17 (4), 818–825. 10.1002/aic.690170410.

Bartholomew, C.H., Pannell, R.B., 1980. The stoichiometry of hydrogen and carbon monoxide chemisorption on alumina-and silica-supported nickel. J. Catal. 65 (2), 390–401. 10.1016/0021-9517(80)90316-4.

Biloen, P., Helle, J.N., van den Berg, F.G., Sachtler, W.M., 1983. On the activity of Fischer-Tropsch and methanation catalysts: A study utilizing isotopic transients. J. Catal. 81 (2), 450–463. 10.1016/0021-9517(83)90183-5.

Borgschulte, A., Gallandat, N., Probst, B., Suter, R., Callini, E., Ferri, D., Arroyo, Y., Erni, R., Geerlings, H., Züttel, A., 2013. Sorption enhanced CO_2 methanation. Phys. Chem. Chem. Phys. 15 (24), 9620–9625. 10.1039/c3cp51408k.

Bremer, J., Sundmacher, K., 2019. Operation range extension via hot-spot control for catalytic CO_2 methanation reactors. React. Chem. Eng. 4 (6), 1019–1037. 10.1039/C9RE00147F.

Bundhoo, A., Schweicher, J., Frennet, A., Kruse, N., 2009. Chemical Transient Kinetics Applied to CO Hydrogenation over a Pure Nickel Catalyst. J. Phys. Chem. C 113 (24), 10731–10739. 10.1021/jp902647z.

Burger, T., Donaubauer, P., Hinrichsen, O., 2020. On the kinetics of the co-methanation of CO and CO_2 on a co-precipitated Ni-Al catalyst. Appl. Catal., B, 119408. 10.1016/j.apcatb.2020.119408.

Currie, R., Nikolić, D., Petkovska, M., Simakov, D.S., 2018. CO_2 Conversion Enhancement in a Periodically Operated Sabatier Reactor: Nonlinear Frequency Response Analysis and Simulation-based Study. Isr. J. Chem. 58 (6-7), 762–775. 10.1002/ijch.201700134.

Dittmeyer, R., Klumpp, M., Kant, P., Ozin, G., 2019. Crowd oil not crude oil. Nat. Commun. 10 (1), 1818. 10.1038/s41467-019-09685-x.

Efstathiou, A.M., Bennett, C.O., 1989. Surface species on Rh/Al_2O_3 during CO/H_2 reaction studied by transient techniques. Chem. Eng. Commun. 83 (1), 129–146. 10.1080/00986448908940658.

Falbo, L., Visconti, C.G., Lietti, L., Szanyi, J., 2019. The effect of CO on CO_2 methanation over Ru/Al_2O_3 catalysts: A combined steady-state reactivity and transient DRIFT spectroscopy study. Appl. Catal., B 256, 117–791. 10.1016/j.apcatb.2019.117791.

Falconer, J.L., Zağli, A.E., 1980. Adsorption and methanation of carbon dioxide on a nickel/silica catalyst. J. Catal. 62 (2), 280–285. 10.1016/0021-9517(80)90456-X.

Fischer, K.L., Freund, H., 2020. On the optimal design of load flexible fixed bed reactors: Integration of dynamics into the design problem. Chem. Eng. J. 393, 124722. 10.1016/j.cej.2020.124722.

Friedland, J., 2018. Charakterisierung eines instationären Reaktionssystems mittels Pulsreaktion am Beispiel der CO-Methanisierung. Doctoral Dissertation, TU Clausthal.

Friedland, J., Kreitz, B., Grimm, H., Turek, T., Güttel, R., 2020. Measuring Adsorption Capacity of Supported Catalysts with a Novel Quasi-Continuous Pulse Chemisorption Method. ChemCatChem. 10.1002/cctc.202000278.

Fujita, S., Terunuma, H., Kobayashi, H., Takezawa, N., 1987. Methanation of carbon monoxide and carbon dioxide over nickel catalyst under the transient state. React. Kinet. Catal. Lett. 33 (1), 179–184. 10.1007/BF02066720.

Fujita, S.-I., Nakamura, M., Doi, T., Takezawa, N., 1993. Mechanisms of methanation of carbon dioxide and carbon monoxide over nickel/alumina catalysts. Appl. Catal., A 104 (1), 87–100. 10.1016/0926-860X(93)80212-9.

Fujita, S.-I., Takezawa, N., 1997. Difference in the selectivity of CO and CO_2 methanation reactions. Chem. Eng. J. 68 (1), 63–68. 10.1016/S1385-8947(97)00074-0.

Fujita, S.-I., Terunuma, H., Nakamura, M., Takezawa, N., 1991. Mechanisms of methanation of carbon monoxide and carbon dioxide over nickel. Ind. Eng. Chem. Res. 30 (6), 1146–1151.

Gałuszka, J., Chang, J.R., Amenomiya, Y. Investigation of Surface Species in the Methanation of Carbon Monoxide on A Supported Nickel Catalyst. Stud. Surf. Sci. Catal. 7, 529–541. 10.1016/S0167-2991(09)60296-2.

Gao, J., Liu, Q., Gu, F., Liu, B., Zhong, Z., Su, F., 2015. Recent advances in methanation catalysts for the production of synthetic natural gas. RSC Adv. 5 (29), 22759–22776. 10.1039/C4RA16114A.

Gao, J., Wang, Y., Ping, Y., Hu, D., Xu, G., Gu, F., Su, F., 2012. A thermodynamic analysis of methanation reactions of carbon oxides for the production of synthetic natural gas. RSC Adv. 2 (6), 2358. 10.1039/c2ra00632d.

Goeppert, A., Czaun, M., Surya Prakash, G.K., Olah, G.A., 2012. Air as the renewable carbon source of the future: an overview of CO_2 capture from the atmosphere. Energy Environ. Sci. 5 (7), 7833. 10.1039/C2EE21586A.

Goodman, D.W., Kelley, R.D., Madey, T.E., Yates Jr, J.T., 1980. Kinetics of the hydrogenation of CO over a single crystal nickel catalyst. J. Catal. 63 (1), 226–234. 10.1016/0021-9517(80)90075-5.

Götz, M., Lefebvre, J., Mörs, F., McDaniel Koch, A., Graf, F., Bajohr, S., Reimert, R., Kolb, T., 2016. Renewable Power-to-Gas: A technological and economic review. Renew. Energy 85, 1371–1390. 10.1016/j.renene.2015.07.066.

Güttel, R., 2013. Study of Unsteady-State Operation of Methanation by Modeling and Simulation. Chem. Eng. Technol. 36 (10), 1675–1682. 10.1002/ceat.201300223.

Güttel, R., Freund, H., Horn, R., Krewer, U., Sauer, J., 2020. Technische Chemie. Nachr. Chem. 68 (6), 46–53. 10.1002/nadc.20204097163.

House, K.Z., Baclig, A.C., Ranjan, M., van Nierop, E.A., Wilcox, J., Herzog, H.J., 2011. Economic and energetic analysis of capturing CO_2 from ambient air. Proc. Natl. Acad. Sci. USA 108 (51), 20428–20433. 10.1073/pnas.1012253108.

Hudgins, R.R., Silveston, P.L., Renken, A., Matros, Y.S., 2013. Introduction, in: Silveston, P.L., Hudgins, R.R. (Eds.), Periodic operation of reactors, 1st ed. Elsevier, Amsterdam, Boston, Kidlington, Oxford, U.K, Waltham, Mass, pp. 1–22.

Inui, T., Funabiki, M., Takegami, Y., 1980. Simultaneous methanation of CO and CO_2 on supported Ni-based composite catalysts. Ind. Eng. Chem. Prod. Res. Dev. 19 (3), 385–388. 10.1021/i360075a018.

Kalz, K.F., Kraehnert, R., Dvoyashkin, M., Dittmeyer, R., Gläser, R., Krewer, U., Reuter, K., Grunwaldt, J.-D., 2017. Future Challenges in Heterogeneous Catalysis: Understanding Catalysts under Dynamic Reaction Conditions. ChemCatChem 9 (1), 17–29. 10.1002/cctc.201600996.

Kiewidt, L., Thöming, J., 2015. Predicting optimal temperature profiles in single-stage fixed-bed reactors for CO_2-methanation. Chem. Eng. Sci. 132, 59–71. 10.1016/j.ces.2015.03.068.

Klusáček, K., Stuchlý, V., 1995. Increasing of carbon monoxide methanation rate by forced feed composition cycling. Catal. Today 25 (2), 169–174. 10.1016/0920-5861(95)00106-P.

Kopyscinski, J., Schildhauer, T.J., Vogel, F., Biollaz, S.M.A., Wokaun, A., 2010. Applying spatially resolved concentration and temperature measurements in a catalytic plate reactor for the kinetic study of CO methanation. J. Catal. 271 (2), 262–279. 10.1016/j.jcat.2010.02.008.

Koschany, F., Schlereth, D., Hinrichsen, O., 2016. On the kinetics of the methanation of carbon dioxide on coprecipitated $NiAl(O)_x$. Appl. Catal., B 181, 504–516. 10.1016/j.apcatb.2015.07.026.

Kreitz, B., Friedland, J., Güttel, R., Wehinger, G.D., Turek, T., 2019a. Dynamic Methanation of CO_2 – Effect of Concentration Forcing. Chem. Ing. Tech. 91 (5), 576–582. 10.1002/cite.201800191.

Kreitz, B., Wehinger, G.D., Turek, T., 2019b. Dynamic simulation of the CO_2 methanation in a micro-structured fixed-bed reactor. Chem. Eng. Sci. 195, 541–552. 10.1016/j.ces.2018.09.053.

Li, X., Li, J., Yang, B., Zhang, Y., 2015. Dynamic analysis on methanation reactor using a double-input–multi-output linearized model. Chin. J. Chem. Eng. 23 (2), 389–397. 10.1016/j.cjche.2014.11.007.

Manchado, M.C., Guil, J.M., Masia, A.P., Paniego, A.R., Menayo, J.M., 1994. Adsorption of H_2, O_2, CO, and CO_2 on a Gamma-Alumina-Volumetric and Calorimetric Studies. Langmuir 10 (3), 685–691. 10.1021/la00015a016.

Marković, A., Seidel-Morgenstern, A., Petkovska, M., 2008. Evaluation of the potential of periodically operated reactors based on the second order frequency response function. Chem. Eng. Res. Des. 86 (7), 682–691. 10.1016/j.cherd.2008.02.003.

Marwood, M., van Vyve, F., Doepper, R., Renken, A., 1994. Periodic operation applied to the kinetic study of CO_2 methanation. Catal. Today 20 (3), 437–448. 10.1016/0920-5861(94)80137-1.

Matros, Y.S., 1987. Unsteady performance of heterogeneous catalytic reactions. React. Kinet. Catal. Lett. 35 (1-2), 425–435. 10.1007/BF02062177.

Meyer, D., Friedland, J., Schumacher, J., Güttel, R., 2021. The Periodic Transient Kinetics Method for Investigation of Kinetic Process Dynamics under Realistic Conditions: Methanation as an Example. Chem. Eng. Res. Des. 173, 253–266. 10.1016/j.cherd.2021.07.011.

Meyer, D., Schumacher, J., Friedland, J., Güttel, R., 2020. Hydrogenation of CO/CO_2 Mixtures on Nickel Catalysts: Kinetics and Flexibility for Nickel Catalysts. Ind. Eng. Chem. Res. 59 (33), 14668–14678. 10.1021/acs.iecr.0c02072.

Miao, B., Ma, S.S.K., Wang, X., Su, H., Chan, S.H., 2016. Catalysis mechanisms of CO_2 and CO methanation. Catal. Sci. Technol. 6 (12), 4048–4058. 10.1039/C6CY00478D.

Mills, G.A., Steffgen, F.W., 1974. Catalytic Methanation. Cat. Rev. 8 (1), 159–210. 10.1080/01614947408071860.

Morimoto, T., Nagao, M., Imai, J., 1971. The adsorption of water on SiO_2, Al_2O_3, and $SiO_2{\cdot}Al_2O_3$. The relation between the amounts of physisorbed and chemisorbed water. Bull. Chem. Soc. Jpn. 44 (5), 1282–1288. 10.1246/bcsj.44.1282.

Mutz, B., Gänzler, A.M., Nachtegaal, M., Müller, O., Frahm, R., Kleist, W., Grunwaldt, J.-D., 2017. Surface oxidation of supported Ni particles and its impact on the catalytic performance during dynamically operated methanation of CO_2. Catalysts 7 (9), 279. 10.3390/catal7090279.

Nikačević, N., Todić, B., Mandić, M., Petkovska, M., Bukur, D.B., 2020. Optimization of forced periodic operations in milli-scale fixed bed reactor for Fischer-Tropsch synthesis. Catal. Today 343, 156–164. 10.1016/j.cattod.2018.12.032.

Polizzotti, R.S., Schwarz, J.A., 1982. Hydrogenation of CO to methane: Kinetic studies on polycrystalline nickel foils. J. Catal. 77 (1), 1–15. 10.1016/0021-9517(82)90140-3.

Raub, A., Karroum, H., Athariboroujeny, M., Kruse, N., 2021. Chemical Transient Kinetics in Studies of the Fischer-Tropsch Reaction and Beyond. Catal. Lett. 151 (3), 613–626. 10.1007/s10562-020-03294-w.

Renken, A., 1972. The use of periodic operation to improve the performance of continuous stirred tank reactors. Chem. Eng. Sci. 27 (11), 1925–1932. 10.1016/0009-2509(72)87051-9.

Rönsch, S., Schneider, J., Matthischke, S., Schlueter, M., Götz, M., Lefebvre, J., Prabhakaran, P., Bajohr, S., 2016. Review on methanation - From fundamentals to current projects. Fuel 166, 276–296. 10.1016/j.fuel.2015.10.111.

Schöß, M.A., Redenius, A., Turek, T., Güttel, R., 2014. Chemische Speicherung regenerativer elektrischer Energie durch Methanisierung von Prozessgasen aus der Stahlindustrie. Chem. Ing. Tech. 86 (5), 734–739. 10.1002/cite.201300086.

Sehested, J., Dahl, S., Jacobsen, J., Rostrup-Nielsen, J.R., 2005. Methanation of CO over nickel: mechanism and kinetics at high H_2/CO ratios. J. Phys. Chem. B 109 (6), 2432–2438. 10.1021/jp040239s.

Shekhtman, S.O., Yablonsky, G.S., 2005. Thin-Zone TAP Reactor versus Differential PFR: Analysis of Concentration Nonuniformity for Gas−Solid Systems. Ind. Eng. Chem. Res. 44 (16), 6518–6522. 10.1021/ie050554g.

Stiegler, T., Meltzer, K., Tremel, A., Baldauf, M., Wasserscheid, P., Albert, J., 2019. Development of a Structured Reactor System for CO_2 Methanation under Dynamic Operating Conditions. Energy Technol. 7 (6), 1900047. 10.1002/ente.201900047.

Stuchlý, V., Klusáček, K., 1993. Unsteady-state carbon monoxide methanation on an Ni/SiO_2 catalyst. J. Catal. 139 (1), 62–71. 10.1006/jcat.1993.1007.

Sutton, D., Kelleher, B., Ross, J.R.H., 2001. Review of literature on catalysts for biomass gasification. Fuel Process. Technol. 73 (3), 155–173. 10.1016/S0378-3820(01)00208-9.

Theurich, S., Rönsch, S., Güttel, R., 2020. Transient Flow Rate Ramps for Methanation of Carbon Dioxide in an Adiabatic Fixed-Bed Recycle Reactor. Energy Technol. 8 (3), 1901116. 10.1002/ente.201901116.

Try, R., Bengaouer, A., Baurens, P., Jallut, C., 2017. Dynamic modeling and simulations of the behavior of a fixed-bed reactor-exchanger used for CO_2 methanation. AIChE J. 38 (5), 2039. 10.1002/aic.15874.

Underwood, R.P., Bennett, C.O., 1984. The COH_2 reaction over nickel-alumina studied by the transient method. J. Catal. 86 (2), 245–253. 10.1016/0021-9517(84)90370-1.

Uribe-Soto, W., Portha, J.-F., Commenge, J.-M., Falk, L., 2017. A review of thermochemical processes and technologies to use steelworks off-gases. Renewable Sustainable Energy Rev. 74, 809–823. 10.1016/j.rser.2017.03.008.

Van Herwijnen, T., 1973. Kinetics of the methanation of CO and CO_2 on a nickel catalyst. J. Catal. 28 (3), 391–402. 10.1016/0021-9517(73)90132-2.

Van Ho, S., 1980. The kinetics of methanation on nickel catalysts. J. Catal. 64 (2), 272–283. 10.1016/0021-9517(80)90502-3.

Vogt, C., Monai, M., Kramer, G.J., Weckhuysen, B.M., 2019. The renaissance of the Sabatier reaction and its applications on Earth and in space. Nat. Catal. 2 (3), 188–197. 10.1038/s41929-019-0244-4.

Weatherbee, G.D., Bartholomew, C.H., 1982. Hydrogenation of CO_2 on group VIII metals: II. Kinetics and mechanism of CO_2 hydrogenation on nickel. J. Catal. 77 (2), 460–472. 10.1016/0021-9517(82)90186-5.

Yadav, R., Rinker, R.G., 1990. An experimental study of methane synthesis by concentration forcing. Chem. Eng. Sci. 45 (11), 3221–3226. 10.1016/0009-2509(90)80214-Y.

Yadav, R., Rinker, R.G., 1992. Step-response kinetics of methanation over a nickel/alumina catalyst. Ind. Eng. Chem. Res. 31 (2), 502–508. 10.1021/ie00002a009.

Zarfl, J., Ferri, D., Schildhauer, T.J., Wambach, J., Wokaun, A., 2015. DRIFTS study of a commercial Ni/γ-Al_2O_3 CO methanation catalyst. Appl. Catal., A 495, 104–114. 10.1016/j.apcata.2015.02.005.

Zimmermann, R.T., Bremer, J., Sundmacher, K., 2020. Optimal catalyst particle design for flexible fixed-bed CO_2 methanation reactors. Chem. Eng. J. 387, 123704. 10.1016/j.cej.2019.123704.